

Effect of Bismuth (Bi) concentration on Bi/Sn electrodes
prepared by electrodeposition in electrochemical reduction of
CO₂ to toward solid carbon products



A Thesis Submitted in Partial Fulfillment of the Requirements
for the Degree of Master of Engineering in Chemical Engineering
Department of Chemical Engineering
FACULTY OF ENGINEERING
Chulalongkorn University
Academic Year 2021
Copyright of Chulalongkorn University

ผลความเข้มข้นของบิสมัทต่อสมบัติของอิเล็กทรอนิกส์/ดิมุกที่เตรียมด้วยการพอกพูนด้วยไฟฟ้า
ในปฏิกิริยารีดักชันทางไฟฟ้าของแก๊สคาร์บอนไดออกไซด์เป็นผลิตภัณฑ์คาร์บอนของแข็ง



วิทยานิพนธ์นี้เป็นส่วนหนึ่งของการศึกษาตามหลักสูตรปริญญาวิศวกรรมศาสตรมหาบัณฑิต
สาขาวิชาวิศวกรรมเคมี ภาควิชาวิศวกรรมเคมี
คณะวิศวกรรมศาสตร์ จุฬาลงกรณ์มหาวิทยาลัย
ปีการศึกษา 2564
ลิขสิทธิ์ของจุฬาลงกรณ์มหาวิทยาลัย

Thesis Title Effect of Bismuth (Bi) concentration on Bi/Sn electrodes
 prepared by electrodeposition in electrochemical
 reduction of CO₂ to toward solid carbon products
By Miss Sarita Phupaichitkun
Field of Study Chemical Engineering
Thesis Advisor Professor JOONGJAI PANPRANOT, Ph.D.

Accepted by the FACULTY OF ENGINEERING, Chulalongkorn University
in Partial Fulfillment of the Requirement for the Master of Engineering

.....
Dean of the FACULTY OF
ENGINEERING
(Professor SUPOT TEACHAVORASINSKUN, D.Eng.)

THESIS COMMITTEE

.....
Chairman
(MERIKA CHANTHANUMATAPORN, D.Eng.)
.....
Thesis Advisor
(Professor JOONGJAI PANPRANOT, Ph.D.)
.....
Examiner
(CHUTIMON SATIRAPIPATHKUL, Ph.D.)
.....
External Examiner
(Assistant Professor Okorn Mekasuwandumrong,
D.Eng.)

จุฬาลงกรณ์มหาวิทยาลัย
CHULALONGKORN UNIVERSITY

สรिता ภูไพจิตรกุล : ผลความเข้มข้นของบิสมัทต่อสมบัติของอิเล็กโทรดบิสมัท/ดีบุกที่เตรียมด้วยการพอกพูนด้วยไฟฟ้าในปฏิกิริยารีดักชันทางไฟฟ้าของแก๊สคาร์บอนไดออกไซด์เป็นผลิตภัณฑ์คาร์บอนของแข็ง. (Effect of Bismuth (Bi) concentration on Bi/Sn electrodes prepared by electrodeposition in electrochemical reduction of CO₂ to toward solid carbon products) อ.ที่ปรึกษาหลัก : ศ. ดร.จุงใจ ปั้นประฉนต

แก๊สคาร์บอนไดออกไซด์ (CO₂) เป็นก๊าซเรือนกระจกหลักที่ทำให้เกิดการเปลี่ยนแปลงสภาพภูมิอากาศ ปฏิกิริยารีดักชันของแก๊สคาร์บอนไดออกไซด์ (CO₂RR) เป็นเทคโนโลยีที่น่าสนใจในการเปลี่ยนแก๊สคาร์บอนไดออกไซด์ด้วยต้นทุนที่ต่ำและเป็นเทคโนโลยีที่ใช้พลังงานไฟฟ้าซึ่งเป็นพลังงานที่ทดแทนได้เป็นแหล่งให้พลังงาน ในงานวิจัยนี้ ศึกษาปฏิกิริยารีดักชันของแก๊สคาร์บอนไดออกไซด์ ไปเป็น ผลิตภัณฑ์คาร์บอนของแข็ง โดยใช้ขั้วไฟฟ้าบิสมัท/ดีบุก (Bi/Sn) ที่เตรียมจากวิธีการพอกพูนทางไฟฟ้า โดยศึกษาผลของความเข้มข้นของบิสมัทที่แตกต่างกันที่ 0.01 M 0.03 M 0.05 M 0.07 M และ 0.1 M ผลการวิเคราะห์สัณฐานวิทยาและความต้านทานการถ่ายโอนประจุของอิเล็กโทรดผ่าน SEM-EDX และ EIS พบว่าอิเล็กโทรด Bi/Sn ที่ความเข้มข้น 0.05 M มีความต้านทานการถ่ายโอนประจุต่ำสุด จึงเป็นตัวเร่งปฏิกิริยาไฟฟ้าที่มีประสิทธิภาพสำหรับการทำ CO₂RR และจากการศึกษาประสิทธิภาพการเร่งปฏิกิริยาของอิเล็กโทรดใน ปฏิกิริยารีดักชันของแก๊สคาร์บอนไดออกไซด์ ภายใต้ระบบอิเล็กโทรไลต์ที่มี [BMIM]BF₄/propylene carbonate/water ที่ศักย์ไฟฟ้าที่ใช้ระหว่าง -1.1 ถึง -1.7 V เทียบกับ Ag/AgCl เพื่อผลิตผลิตภัณฑ์คาร์บอน โดยทำการวิเคราะห์ผลิตภัณฑ์ที่เป็นของแข็ง ของเหลว และก๊าซโดย Raman spectroscopy, NMR และ GC ตามลำดับ และผลจากกล้องจุลทรรศน์อิเล็กตรอนแบบส่องผ่านยังแสดงให้เห็นว่าผลิตภัณฑ์คาร์บอนของแข็งมีลักษณะเป็นพอลิคริสตัลไลน์แกรไฟีน สภาวะที่มีความเหมาะสมที่สุดสำหรับปฏิกิริยารีดักชันของแก๊สคาร์บอนไดออกไซด์ ในการผลิตผลิตภัณฑ์คาร์บอนของแข็ง โดยใช้ขั้ว Bi/Sn ภายใต้ระบบอิเล็กโทรไลต์ [BMIM]BF₄/PC/DI อิเล็กโทรด คือที่ความเข้มข้นของบิสมัท 0.05 M และศักย์ไฟฟ้าที่ใช้ -1.3 V เทียบกับ Ag/AgCl



สาขาวิชา วิศวกรรมเคมี
ปีการศึกษา 2564

ลายมือชื่อนิสิต
ลายมือชื่อ อ.ที่ปรึกษาหลัก

6272090721 : MAJOR CHEMICAL ENGINEERING

KEYWORD Electrochemical carbon dioxide reduction, Bismuth electrode,
D: Electrodeposition, Carbon production

Sarita Phupaichitkun : Effect of Bismuth (Bi) concentration on Bi/Sn electrodes prepared by electrodeposition in electrochemical reduction of CO₂ to toward solid carbon products. Advisor: Prof. JOONGJAI PANPRANOT, Ph.D.

Carbon dioxide (CO₂) is the main greenhouse gas that contributes to climate change. The electrochemical carbon dioxide reduction (CO₂RR) is an interesting and low-cost CO₂ conversion technology using renewable electricity as an energy source. Herein, CO₂RR to solid carbon products was studied on bismuth/tin (Bi/Sn) electrodes synthesized by electrodeposition method. Different Bi concentration (0.01 M, 0.03 M, 0.05 M, 0.07 M and 0.1 M) were used to prepare the electrodes by electrodeposition method. The SEM-EDX and EIS results which reveal that the Bi/Sn electrode prepared in 0.05 M Bi³⁺ had the lowest charge transfer resistance and was indicated as a CO₂RR promising effective electrocatalyst. The catalytic performances of the electrodes in CO₂RR were examined under an electrolyte system containing [BMIM]BF₄/propylene carbonate/water at the applied potential between -1.1 to -1.7 V vs. Ag/AgCl to produce carbon products. Raman spectroscopy, NMR, and GC were used to analyze the solid, liquid, and gaseous products, respectively. From TEM results, the solid carbon products were identified as polycrystalline graphene. The proper bismuth structures and suitable reaction conditions for CO₂RR to solid carbon products on the Bi/Sn electrocatalysts were obtained at 0.05 M Bi³⁺ and -1.3 V vs. Ag/AgCl, respectively.



Field of Study: Chemical Engineering

Student's Signature

Academic 2021

Advisor's Signature

Year:

.....

ACKNOWLEDGEMENTS

The completion of this thesis could not have been possible without the participation and support of so many people, whose names may not all be enumerated. Their contributions are sincerely appreciated and truly acknowledged. However, I would like to express my sincere gratitude, particularly to the following:

Professor Ph.D. Joongjai Panpranot, my advisor, for giving support, valuable guidance and advice, as well as motivation. And D. Piriya Pinthong, my senior, for giving valuable guidance and advice.

Furthermore, D. Merika Chanthanumataporn as the chairman, and Ph.D. Chutimon Satirapipathkul, and Asst. Prof. D. Okorn Mekasuwandumrong, as the thesis committees, for their helpful comments and suggestions on this thesis.

To all relatives, friends, and others who in one way or another shared their support and kindness, thank you.

Finally, the Financial supports from the MalaysiaThailand Joint Authority (MTJA) Research Cess Fund and the National Research Council of Thailand (NRCT) is gratefully acknowledged.

Sarita Phupaichitkun

TABLE OF CONTENTS

	Page
.....	iii
ABSTRACT (THAI)	iii
.....	iv
ABSTRACT (ENGLISH)	iv
ACKNOWLEDGEMENTS	v
TABLE OF CONTENTS	vi
LIST OF TABLES	viii
LIST OF FIGURES	ix
CHAPTER I	1
INTRODUCTION	1
1.1 Introduction	1
1.2 Objectives of the Research	3
1.3 Scope of the Research	4
CHAPTER II	5
BACKGROUND AND LITERATURE REVIEWS	5
2.1 Carbon dioxide (CO ₂)	5
2.2 Electrochemical reduction of CO ₂ (CO ₂ RR)	6
2.3 The study of electrode	9
2.4 Electrodeposition	11
2.5 Ionic liquid	13
2.6 Bi electrocatalysts	19
CHAPTER III	26
MATERIALS AND METHODS	26
3.1 Materials	26
3.2 Catalysts preparation	27

3.2.1 Preparation of Sn electrode	27
3.2.2 Preparation of Bi/Sn electrode	27
3.3 Catalyst Characterization.....	28
3.4 H-type cell preparation	28
3.5 Effect of Bi concentration on the properties of electrocatalyst	29
3.6 Effect of potentials on electrocatalytic performance	32
3.7 Stability test of electrocatalyst.....	33
3.8 Research methodology	33
CHAPTER IV	35
RESULTS AND DISCUSSIONS.....	35
4.1 Characterization of Bi/Sn electrode with various concentrations	35
4.2 LSV of electrocatalysts prepared in various Bi concentrations bath.....	40
4.3 EIS with various Bi concentrations	40
4.4 CO ₂ RR performance test on electrocatalysts prepared in various Bi concentrations bath.....	42
4.5 Potential for the CO ₂ RR at 70 min.....	50
4.6 The stability test of CO ₂ RR on 0.05Bi/Sn electrode for 150 min.	53
CHAPTER V	56
CONCLUSIONS.....	56
REFERENCES	59
VITA.....	66

LIST OF TABLES

	Page
Table 1. The equilibrium potentials (E°) of CO ₂ reduction and HER [1, 16, 36].....	8
Table 2. Noble metal in CO ₂ RR	17
Table 3. Post-transition metal in CO ₂ RR.....	18
Table 4. Bi electrocatalyst in the CO ₂ RR	19
Table 5. The materials and chemicals used in the electrodeposition method.....	26
Table 6. The materials and chemicals used in the CO ₂ RR.	26
Table 7. The operating conditions of GC.....	31
Table 8. EDX results of 0.01-0.1 M Bi on Sn electrode.....	37
Table 9. Charge-transfer resistances of Bi/Sn electrocatalyst prepared in several Bi concentration bath.....	42
Table 10. The EDX result after CO ₂ RR at -1.1 V for 70 min.....	43
Table 11. TEM-EDX results of Bi/Sn electrode after CO ₂ RR at -1.1 V for 70 min ..	47
Table 12. The EDX result of 0.05 Bi/Sn electrode after CO ₂ RR for 70 min.....	51
Table 13. The gas products of CO ₂ RR on 0.05Bi/Sn electrode at various applied potentials for 70 min.	51
Table 14. The EDX result after CO ₂ RR at 0.05 Bi/Sn -1.3 V.....	53
Table 15. The gas products of CO ₂ RR on 0.05Bi/Sn electrode at -1.3 V for 150 min.	54

LIST OF FIGURES

	Page
Figure 1. The electrochemical reaction of CO ₂ cells.[36]	6
Figure 2. Electrochemical reduction of CO ₂ [1]	7
Figure 3. Homogeneous Electrocatalysis [1]	9
Figure 4. Heterogeneous electrocatalysis of CO ₂ RR in aqueous systems [38].....	10
Figure 5. Electrodeposition step [39].....	11
Figure 6. Compare electrolytes in CO ₂ RR [18].....	14
Figure 7. The structure of the ionic liquid [1].....	15
Figure 8. The mechanism of ionic liquid in CO ₂ RR to CO [42]	15
Figure 9. The mechanism of ionic liquid in CO ₂ RR to carbon product [16].....	16
Figure 10. Electrodeposition of Bi catalysts on Sn electrode	27
Figure 11. H-type cell preparation	28
Figure 12. LSV experiment.....	29
Figure 13. EIS experiment	30
Figure 14. CO ₂ RR performance at -1.1 volt	31
Figure 15. CO ₂ RR performance by varied potentials	32
Figure 16. SEM images of Sn electrode: (a) Sn electrode (b) Sn electrode after mechanically polishing	35
Figure 17. SEM images of Bi/Sn electrode : (a) 0.01 M (b) 0.03 M (c) 0.05 M (d) 0.07 M and (e)0.1 M Bi/Sn electrode	36
Figure 18. 0.05 M Bi/Sn electrode cross-section by SEM.....	38
Figure 19. Bi/Sn electrodes prepared by electrodeposition of Bi ³⁺ on Sn foil	38
Figure 20. Bi 4f XPS spectra image of Bi/Sn electrode by electrodeposition.....	39
Figure 21. LSV result of Bi/Sn electrode.....	40
Figure 22. EIS result of Bi/Sn electrode	41
Figure 23. SEM images after CO ₂ RR at -1.1 V : (a) 0.01 M (b) 0.03 M (c) 0.05 M (d) 0.07 M and (e) 0.1 M Bi concentration on Sn electrode	42

Figure 24. NMR result of electrolyte: (a) 13 CNMR (b) 1 HNMR	43
Figure 25. NMR result of all concentrations: (a) 13 CNMR (b) 1 HNMR	43
Figure 26. Raman results of the Bi/Sn electrodes after CO ₂ RR reaction at -1.1 V vs. Ag/AgCl for 70 min	44
Figure 27. TEM : (a) 0.01 M (b) 0.03 M (c) 0.05 M (d) 0.07 M (e) 0.1 M Bi/Sn electrode after CO ₂ RR at -1.1 V vs. Ag/AgCl for 70 min	45
Figure 28. TEM-EDX results : (a) 0.01 M (b) 0.03 M (c) 0.05 M (d) 0.07 M (e) 0.1 M Bi/Sn electrode after CO ₂ RR at -1.1 V vs. Ag/AgCl for 70 min	46
Figure 29. Bi 4f XPS spectra image of Bi/Sn electrodes after CO ₂ RR at -1.1 V	48
Figure 30. C1s XPS spectra image of the Bi/Sn electrodes after CO ₂ RR at -1.1 V ..	49
Figure 31. SEM images of 0.05 Bi/Sn after CO ₂ RR for 70 min : (a)-1.1 V (b) -1.3 V (c) -1.5 V (d) -1.7 v	50
Figure 32. Raman results of the 0.05Bi/Sn electrode after CO ₂ RR reaction at -1.1 to -1.7 V vs. Ag/AgCl for 70 min by using 0.05 M Bi/Sn electrode	52
Figure 33. SEM image of 0.05 Bi/Sn after CO ₂ RR (a) 70 min (b) 150 min.....	53
Figure 34. Raman results of the Bi/Sn electrodes after CO ₂ RR reaction at -1.3 V vs. Ag/AgCl for 70 and 150 min by using 0.05 M Bi/Sn electrode	54

CHAPTER I

INTRODUCTION

1.1 Introduction

The rising level of greenhouse gases is now driving the change in the Earth's climate that causes natural disasters such as flooding, drought, wildfire, and storm surge. The primary greenhouse gas is carbon dioxide (CO₂), an inexpensive, non-toxic, inert gas, which has been released into the atmosphere through burning fossil fuels (coal, natural gas, and oil), solid waste, trees, and other biological materials, and also a result of specific chemical reactions causing the greenhouse effect and environmental issues. However, CO₂ can be used as an initial substance in producing alcohol, acids, and other chemicals. In recent years, the interest has been growing in reducing CO₂ and changing it into fuels and other value-added chemical products [1, 2].

There are several CO₂ conversion technologies such as thermal, photochemical, enzymatic, and electrochemical processes. Nevertheless, the thermal catalytic reactions are unfavourable and need harsh reaction conditions due to the non-reactive properties of inert gases. In photocatalytic reactions, the efficiency is low [1, 2]. And the enzymatic process, the process is slow from using multistep processes, unstable catalysts, complex regeneration, and discontinuous process [3]. Among these, electrochemical reduction is a superior technology for carbon dioxide reduction due to its high efficiency, simple operation, mild conditions, and potential opportunities for large-scale practical applications.

Bismuth (Bi) is an attractive electrocatalyst metal because it is a stable, non-toxic metal with low price, minimal environmental impact, and high selectivity of CO production in CO₂RR [4, 5]. There are various methods to prepare electrodes, such as pulsed laser deposition, vacuum thermal evaporation, melt spinning, electrodeposition, etc [6]. Pulsed laser deposition is a high-quality thin film but expensive and may not be helpful for fabricating large-scale uniform coatings [7]. Vacuum thermal evaporation is of very high purity. Nevertheless, it has a non-uniform thickness on complex surfaces and is expensive [8]. The melt spinning

technique is fast and cheapest however, the properties of the sample may change with time, and the thickness of samples is inhomogeneous by area [9]. The electrodeposition method is commonly used in the preparation of electrodes in advance that combines low costs and the ability to fast cover large complex surfaces [6]. Several Bi electrodes have been studied in CO₂RR [4-6, 8, 10, 11]. Bi–Tin (Sn) alloy electrode [9, 12-15], Bi/Sn electrode [16], and Sn electrode [1, 2, 17] were also studied in the electrochemical reduction of CO₂ because of low cost, low toxicity, and high-efficiency [17].

To improve the efficiency of CO₂RR, the use of ionic liquid electrolyte is of interest because it was found to increase the efficiency due to strong absorption capacity and unique properties of zero vapour pressure, high electrical conductivity, high thermal stability, high gas solubility, and expansive electrochemical windows [1, 4, 5]. Meanwhile, other electrolytes, such as aqueous ones, have low CO₂ solubility and often lead to hydrogen evolution [18]. Organic electrolytes increase CO₂ solubility but poor conductivity and environmental problems from large volatilization [1]. The effects of ionic liquid as an electrolyte in CO₂RR have been studied by changing types of ions [4, 5, 11, 19, 20] or combining the ionic liquid with aqueous electrolytes or organic electrolytes or both electrolytes in different ratios [20-22].

The products from the electrochemical carbon dioxide reduction (CO₂RR) range from carbon monoxide (CO), formate (HCOOH), methanol (CH₃OH) methane (CH₄), and ethanol (C₂H₅OH), to solid carbon (C) [1, 2, 16]. Generally, the attractive product in CO₂RR is CO because it can combine with the H₂ produced from the water–gas shift reaction in the Fischer–Tropsch (FT) synthesis in the form of syngas (CO and H₂) to produce synthetic petroleum and other liquid fuels [22]. Recently, carbon allotropes such as graphene are an interesting product from CO₂RR because of their technically desirable properties to revolutionary materials (e.g., high electrical/thermal conductivity, high strength, lightweight, and bio-compatibility) that can be used in the fields of electronics, optics, bioengineering, biomedical, tribology, etc [16]. However, there has been few research about carbon products produced from CO₂RR compared to CO [16, 23, 24].

Previous research by Rungkiat et al. 2022, CO₂RR was studied using 0.1 M Bi deposited on Sn electrode (Bi/Sn) by electrodeposition in a ternary electrolyte system

comprising of 1-Butyl-3-methylimidazolium tetrafluoroborate ([BMIM]BF₄), propylene carbonate (PC or ethylene glycol), and de-ionized water (DI) at -1.1 V for 70 min. The results showed that the reaction did not produce any liquid product, and carbon allotropes were obtained as the main products from the reaction [16]. However, the electrodeposition and also CO₂RR conditions are needed to be further investigated to improve the electrocatalytic efficiency of the Bi/Sn electrodes in [BMIM]BF₄/ PC/DI.

Several studies showed an improved efficiency of electrocatalysts prepared by the electrodeposition method in CO₂RR by varying deposition time and concentration [25, 26]. The longer deposition time led to the formation of a thicker layer, and a high current was inclined to make a dendrite cluster with an outsized size, thus covering the surface of the substrate. Notably, the rise of deposition time led to the enlargement of apparent pore size. This might be attributed to slow rates of hydrogen evolution in conjunction with bubble coalescence in such conditions [27]. Increasing concentration also produced nuclei with a coarser texture that was bigger and taller. But at the surface area, it will lower population density than the lower concentration that gave deposits with a relatively large surface area [28].

Therefore, this research aims to study the effect of Bi concentrations on the characteristics and performances of the Bi/Sn electrode prepared by electro-deposition in the CO₂RR under the [BMIM]BF₄/ PC/DI system.

1.2 Objectives of the Research

To study the effect of Bi concentrations on the characteristics and performances of the Bi/Sn electrode prepared by electrodeposition in the CO₂RR under the 1-Butyl-3-methylimidazolium tetrafluoroborate ([BMIM]BF₄)/ propylene carbonate (PC)/ deionized water (DI) system.

1.3 Scope of the Research

1.3.1 Electrode Preparation

- Bi/Sn electrode was prepared by electrodeposition of Bi on the Sn substrate.
- The concentration of Bi^{3+} were 0.01, 0.03, 0.05, 0.07, and 0.1 M at -0.7 V for 10 min.

1.3.2 Ionic electrolytes: The anolyte was Potassium bicarbonate (KHCO_3) in an aqueous solution and the catholyte was the mixture of propylene carbonate (PC), [BMIM] BF_4 , and deionized water (DI).

1.3.3 Study and characterization

- The CO_2RR was tested at the potential of -1.1, -1.3, -1.5, and -1.7 V vs. Ag/AgCl for 70 min.
- The condition with highest performance was further investigate the stability for 150 min.
- A potentiostat (Metrohm Autolab): was used for the electrodeposition method, Linear sweep voltammetry (LSV), Electrochemical impedance spectroscopy (EIS), and the CO_2RR experiments.
- The catalysts: Bi/Sn electrodes were characterized by Scanning electron microscope-energy dispersive X-ray spectroscopy (SEM-EDX), X-ray photoelectron spectroscopy (XPS), and TEM-EDX-SAED (Trans-mission Electron Microscopy, Energy-dispersive X-ray spectroscopy, and Selected Area Electron Diffraction).
- The products of CO_2RR were characterized by Gas chromatography (GC), Nuclear magnetic resonance (NMR), and Raman spectroscopy.

CHAPTER II

BACKGROUND AND LITERATURE REVIEWS

2.1 Carbon dioxide (CO₂)

Carbon dioxide (CO₂) is a key carbon source for sustaining life on Earth. Nevertheless, it is the main greenhouse gas that enables the caging of heat in our atmosphere by regulating the temperature of the atmosphere and the planet. Generally, the concentration of CO₂ in the atmosphere is approximately 203 gigatons of CO₂ are recycled each year by controlled by photosynthetic organisms and geological phenomena. Due to current human activities, fossil fuel usage generates more than 30 gigatons of added CO₂ per year, which cannot be accommodated in the natural carbon cycle. Therefore, CO₂ levels in the atmosphere have risen considerably in the last 100 years, and the following greenhouse effect has hugely impacted climate change [29]. According to NASA's temperature data, the Earth was about 1.9 degrees Fahrenheit (or about 1.1 degrees Celsius) in 2021, warmer than on average in the 19th-century, when the industrial revolution began [30]. The start of extreme heatwaves will become widespread when Earth's temperature warms to 1.5 °C, which around 14% of the world's population will be affected by severe heatwaves at least once every five years, while at 2 °C, that percentage of the affected population will rise to 37% [31]. On November 13, 2021, at the COP26 meeting in Glasgow, all countries made an agreement on the Glasgow Climate Pact to keep 1.5 °C alive, and Paris Agreement asked countries to come forward with ambitious 2030 emissions reduction goals that align with reaching net zero by the center of the century [32]. As a consequence, developing methods and researches in order to reduce CO₂ aggregation in the environment is critical. Meanwhile, reducing or converting CO₂ to be useful chemical products can claim to be carbon credit (\$4.73 per credit in 2021) and reduce CO₂ aggregation in the environment is critical [33].

CO₂ properties are colorless, odorless, nonflammable gas with a slightly sour flavor, with a linear and centrosymmetric molecule. Although the C=O bonds in CO₂ are polar as oxygen has a stronger electronegativity than carbon, causing the electron fog to approach towards O, the molecule's net dipole moment is zero since the two

bond dipoles neutralize each other out due to the linear structure. The carbon core of the CO₂ molecule is electrophilic, and gaseous carbon dioxide is not very reactive at normal temperatures. Because of the C=O bond energy of 805 kJ mol⁻¹, the carbon dioxide molecule is relatively stable and does not easily break down into simpler compounds. On the other hand, high temperatures, ultraviolet light, or electrical discharge may affect some decomposition [34, 35].

2.2 Electrochemical reduction of CO₂ (CO₂RR)

An overall electrochemical process comprises cathodic and anodic processes that occur in two sections separated by a membrane to prevent the blending of cathodic and anodic reaction products. The cathodic or anodic components of the process relate to electron-conducting phases (electrodes) joined by an ion-conducting phase (electrolyte medium) [1, 29, 34].

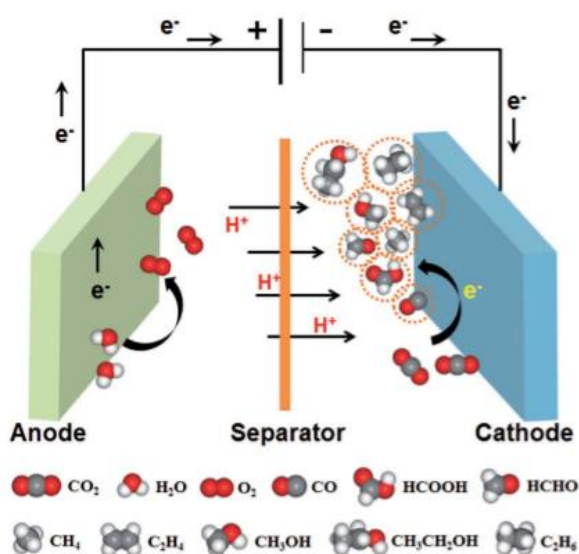


Figure 1. The electrochemical reaction of CO₂ cells.[36]

CO₂RR is a multi-electron/proton transfer process with the following five steps: (1) CO₂ dissolution, (2) CO₂ adsorption on the catalyst surface, (3) one-electron reduction of CO₂ to CO₂⁻ free radical (CO₂^{*-}), (4) additional electron/proton transfer for target product production, and (5) product desorption into the electrolyte or gaseous product escape from the electrolyte. Although the products of the

electrochemical reduction can be controlled by modifying reaction parameters, including the electrolyte, electrode, electrocatalyst, and an applied voltage, an efficient and selective CO₂RR is not straightforward due to the chemical inertness of CO₂ molecules. A large overpotential is frequently needed to improve the kinetically sluggish [1, 29, 34].

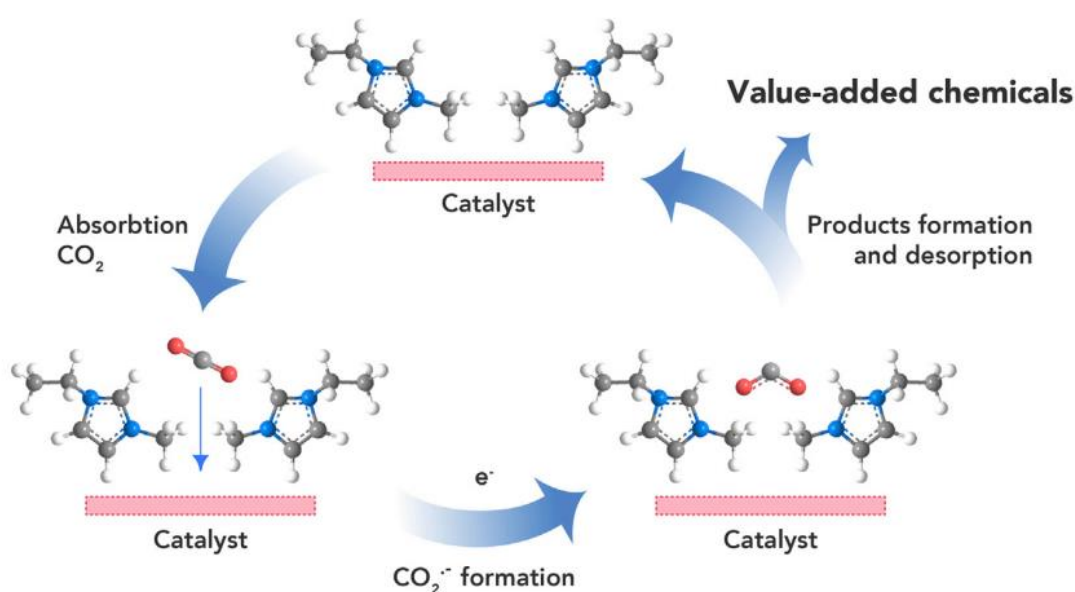


Figure 2. Electrochemical reduction of CO₂ [1]

By using the electroreduction of CO₂ pathways, CO₂ may be converted into small carbonaceous molecules with a high energy density, such as carbon monoxide (CO), formic acid/formate (HCOOH/HCOO⁻), methanol (CH₃OH), methane (CH₄), acetic acid (CH₃COOH), carbon, and so forth. From a thermodynamic study, a variety of half-reactions and their corresponding electrode potentials versus standard hydrogen electrode (SHE) in aqueous solution (pH = 7, at 25 °C, 1 atm, and 1.0 m concentration of other solutes) or the equilibrium potentials (E^o) of CO₂ reduction and HER are shown in Table 1 [1, 16, 36].

Table 1. The equilibrium potentials (E^0) of CO_2 reduction and HER [1, 16, 36]

Electrochemical Reduction	E^0 (V versus SHE)
$\text{CO}_2(\text{g}) + \text{e}^- \rightarrow \text{CO}_2^{*-}$	-1.900
$\text{CO}_2(\text{g}) + 2\text{H}_2\text{O}(\text{l}) + 4\text{e}^- \rightarrow \text{C}(\text{s}) + 4\text{OH}^-$	-0.627
$\text{CO}_2(\text{g}) + 2\text{H}^+ + 2\text{e}^- \rightarrow \text{HCOOH}(\text{l})$	-0.610
$\text{CO}_2(\text{g}) + \text{H}_2\text{O}(\text{l}) + 2\text{e}^- \rightarrow \text{HCOO}^-(\text{aq}) + \text{OH}^-$	-0.430
$\text{CO}_2(\text{g}) + 2\text{H}^+ + 2\text{e}^- \rightarrow \text{CO}(\text{g}) + \text{H}_2\text{O}(\text{l})$	-0.530
$\text{CO}_2(\text{g}) + \text{H}_2\text{O}(\text{l}) + 2\text{e}^- \rightarrow \text{CO}(\text{g}) + 2\text{OH}^-$	-0.520
$\text{CO}_2(\text{g}) + 4\text{H}^+ + 2\text{e}^- \rightarrow \text{HCHO}(\text{l}) + \text{H}_2\text{O}(\text{l})$	-0.480
$\text{CO}_2(\text{g}) + 3\text{H}_2\text{O}(\text{l}) + 4\text{e}^- \rightarrow \text{HCHO}(\text{l}) + 4\text{OH}^-$	-0.890
$\text{CO}_2(\text{g}) + 6\text{H}^+(\text{l}) + 6\text{e}^- \rightarrow \text{CH}_3\text{OH}(\text{l}) + \text{H}_2\text{O}(\text{l})$	-0.380
$\text{CO}_2(\text{g}) + 5\text{H}_2\text{O}(\text{l}) + 6\text{e}^- \rightarrow \text{CH}_3\text{OH}(\text{l}) + 6\text{OH}^-$	-0.810
$\text{CO}_2(\text{g}) + 8\text{H}^+ + 8\text{e}^- \rightarrow \text{CH}_4(\text{g}) + 2\text{H}_2\text{O}(\text{l})$	-0.240
$\text{CO}_2(\text{g}) + 6\text{H}_2\text{O}(\text{l}) + 8\text{e}^- \rightarrow \text{CH}_4(\text{g}) + 8\text{OH}^-$	-0.250
$2\text{CO}_2(\text{g}) + 72\text{H}^+ + 12\text{e}^- \rightarrow \text{C}_2\text{H}_4(\text{g}) + 4\text{H}_2\text{O}(\text{l})$	0.0600
$2\text{CO}_2(\text{g}) + 8\text{H}_2\text{O}(\text{l}) + 12\text{e}^- \rightarrow \text{C}_2\text{H}_4(\text{g}) + 12\text{OH}^-$	-0.340
$2\text{CO}_2(\text{g}) + 12\text{H}^+ + 12\text{e}^- \rightarrow \text{CH}_3\text{CH}_2\text{OH}(\text{l}) + 3\text{H}_2\text{O}(\text{l})$	0.0800
$2\text{CO}_2(\text{g}) + 9\text{H}_2\text{O}(\text{l}) + 12\text{e}^- \rightarrow \text{CH}_3\text{CH}_2\text{OH}(\text{l}) + 12\text{OH}^-(\text{l})$	-0.330
$2\text{H}^+ + 2\text{e}^- \rightarrow \text{H}_2(\text{g})$	-0.420

The rearrangement of a linear molecule to a bent radical anion (CO_2^{*-}) in CO_2 reduction needs a large amount of energy occurring at -1.90 V versus the standard hydrogen electrode (SHE). Although the CO_2^{*-} radical obtained is highly reactive and can form target products after several protons and electron transfer approaches, it is challenging to convert CO_2 to the desired product with high efficiency and selectivity by commonly used electrode materials in aqueous electrolytes. Additionally, a larger negative potential is needed to drive this reaction than E^0 , which implies the high overpotential is primarily due to the first phase of CO_2 electroreduction [1].

The performance of CO_2RR was evaluated using the Faradaic efficiency (FE), which was calculated as an equation [37, 38].

$$FE(\%) = (anF/Q)*100$$

where F is the Faraday constant ($F = 96,485 \text{ C mol}^{-1}$), a is the number of transferred electrons, n is the amount of the particular product (mol), and Q is the charge quantity that is consumed in the reduction (C) [37, 38].

2.3 The study of electrode

Homogeneous and heterogeneous catalytic processes can improve CO₂RR efficiency. Homogeneous electrocatalysts are micro cyclic organics or metalorganic complexes possessing highly accessible metal active sites. The CO₂RR homogeneous catalysis has been widely studied since the 1970s, but because of the high cost, toxicity, and complicated separation, it may be unable to be used in industry. On the other hand, Heterogeneous electrocatalysis has attracted much interest in recent years due to its low cost and environmentally friendly features. In the CO₂RR, the approaches for nano-catalyst production are complex, referring to the oxygen reduction reaction (ORR), oxygen evolution reaction (OER), and hydrogen evolution reaction (HER). Therefore, many studies will focus on heterogeneous electrode materials in this section [1, 38].

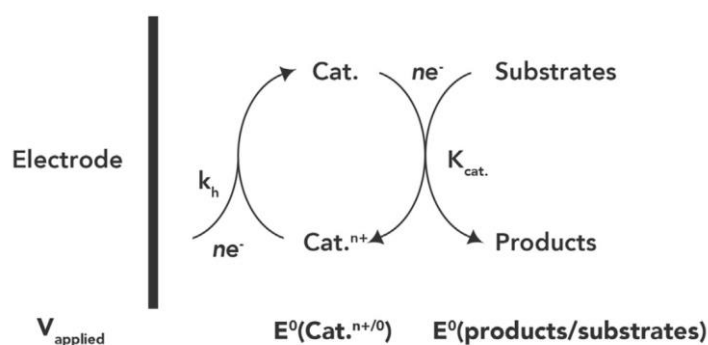


Figure 3. Homogeneous Electrocatalysis [1]

The heterogeneous electrocatalysts mechanisms of metal electrodes are summarized in Figure 4. Polycrystalline metal electrodes may be categorized into three types based on their tendency to bind intermediates. The first group, consisting of Hg, Pb, Bi, Sn, and In, prefers to attach to the *OCHO intermediate and benefits the production of formic acid or formate. The second group, Au, Ag, Zn, and Pd, may

strongly bind the $^*\text{COOH}$ intermediate following a protonation step from the CO_2^{*-} intermediate, removing the H_2O molecule to form $^*\text{CO}$ intermediate. Nonetheless, the binding between these metals and the $^*\text{CO}$ intermediate is insufficiently strong and cannot promote further reduction, resulting in CO being released from the metal catalysts' surface. And in the third group, Cu is the only metal in this group because of its high binding energy to stabilize $^*\text{CO}$, which is advantageous for more $^*\text{CO}$ reduction and producing value-added products like hydrocarbons and alcohols. In the third group, Cu is the only metal in this group because of its high binding energy to stabilize $^*\text{CO}$ which is advantageous for more $^*\text{CO}$ reduction and producing value-added products like hydrocarbons and alcohols. Other metals, such as Pt , Ni , Fe , and Ti , are more likely to bind hydrogen than carbon intermediates, causing the preferential selectivity of HER and the suppression of CO_2RR . Hence, the metal-to-intermediate binding energy is a major determinant of high selectivity and effective CO_2RR performance [38].

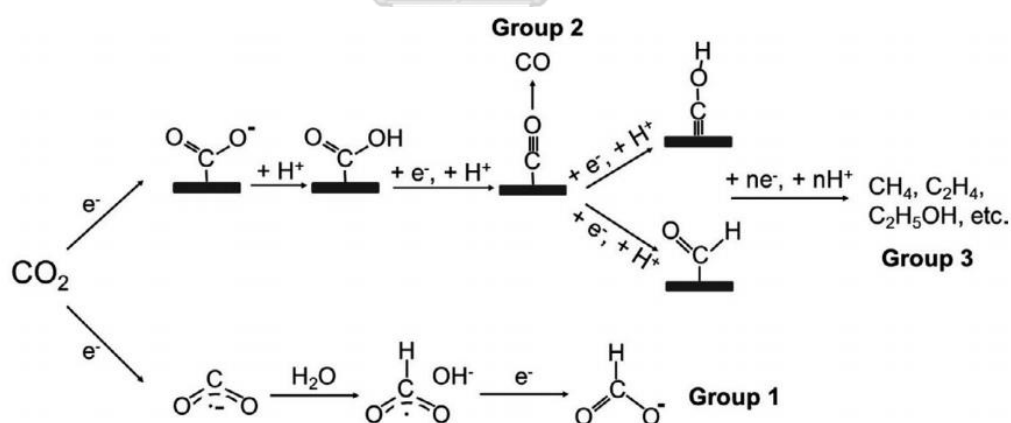


Figure 4. Heterogeneous electrocatalysis of CO_2RR in aqueous systems [38]

Many catalysts of the heterogeneous electrocatalysts have been exploited, including metal catalysts, metal oxides, metal chalcogenides, and metal-free catalysts. The heterogeneous electrocatalysts are low-cost and easily recyclable for large-scale

applications. In this case, CO₂ reduction mainly occurs at the interface of the electrolytes and heterogeneous electrocatalysts because the electrocatalysts are usually solid and the electrolytes are solvents saturated with CO₂ [1].

2.4 Electrodeposition

Electrodeposition is a material production technology using an applied potential or current flowing through an electrolytic solution containing metal ions. Electrochemical deposition is a low-cost and effective way to rapidly cover large, complex surfaces. As demonstrated by the electrodeposition mechanism in Figure 5, in an electrically conducting substrate, these metal ions are reduced to atoms, resulting in metals, alloys, metal-based compounds, or composites as a coating or powder form. In the presence of an applied potential, mass transfer of ions towards the cathode occurs via three distinct processes. Firstly, convection (macroscopic motion of the fluid due to stirring, density gradients originating from eddies, or hydrodynamic transport) Secondly, diffusion (ion motion due to gradients in chemical potential, usually concentration gradients). And lastly, migration (motion of the ions due to an applied electric field). Metal ions in the bulk electrolyte are bonded to water molecules by ion-dipole forces, whereas they are bound to complex molecules via dipole or covalent interactions [6, 39].

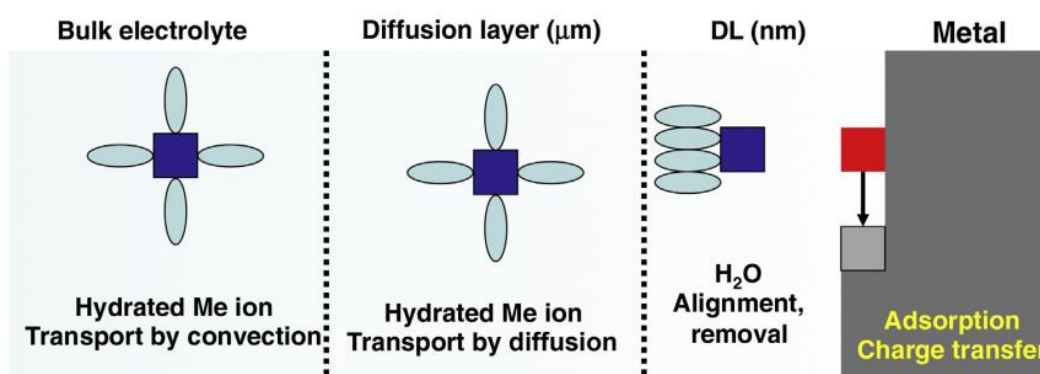
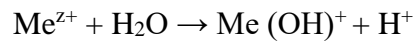


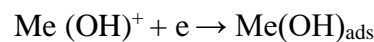
Figure 5. Electrodeposition step [39]

Three major processes are involved in the electrodeposition of these metals in electrolytes. In the first phase of convection, the metal ion interacts strongly with

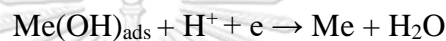
water to generate a metal monohydroxide. A dynamic equilibrium is achieved overtime where the rate of metal dissolution from the electrode equals the rate of metal ion reduction when a metal Me is immersed in a solution containing the corresponding ion Me^{z+} [39].



The second phase is diffusion, in which a metal monohydroxide is reduced and adsorbs at the electrode [39].



Furthermore, in the last phase of migration, the metal is reduced by the mediated hydrogen ion [39].



Accordingly, the overall reaction is composed of two equations in the electro-deposition: the ion metal reduction equation and the water oxidation reaction [40].



The amount of metal deposit can be computed using equations 1, 2, and 3 by which the quantity of metal deposited (W) at the cathode surface can be expressed as the product of the quantity of total coulombs passed (Q_c) and the electrochemical equivalent of the metal (z_c) [40]:

$$Q_c = \int I \delta t \tag{1}$$

$$z_c = M_w / nF \tag{2}$$

$$W = \int I \delta t M_w / nF \tag{3}$$

where I is the current applied over a period of time t, M_w is the molar mass of the metal that undergoes electroreduction, n number of electrons and F is the Faraday constant. Electrodeposition reactions that are heterogeneous take place in the cathode/electrolyte interfacial region which involves the mass transfer and charge transfer steps . The rate-limiting step of electrodeposition reaction is determined by the slowest step as the rate of reduction, and also the cathodic current [40].

2.5 Ionic liquid

The electrolyte in CO₂RR are commonly ionic liquid, aqueous electrolytes, and organic electrolytes. In aqueous electrolyte, a solubility of CO₂ in aqueous electrolyte 0.033 mol⁻¹ was measured under conditions (298 K, 1 atm), resulting in low conversion efficiency of CO₂ reduction. Besides, due to the formation of CO₂^{*-} radical, the sluggish kinetics is the reaction's main energy barrier. Therefore, sufficient large overpotentials are frequently needed to drive this reaction. Also, the HER, extensively in aqueous media, is another complicating factor. As a competitive response, it can decrease the selectivity of the target product. Furthermore, most researchers concentrated on weakly acidic or alkaline CO₂-saturated aqueous solutions containing inorganic salts such as anions, HCO₃⁻, SO₄²⁻, Cl⁻, Br⁻, I⁻; alkali metal cations, K⁺ and Na⁺. And the catalytic activity and product selectivity are improved, although the exact mechanism is still under discussion. Despite the fact that there are still challenging challenges with CO₂ reduction, CO₂ in aqueous electrolytes might undergo C–C coupling and be further reduced to multi-carbon compounds. Hence, the selectivity and variety of the products can be enhanced by designing effective catalysts for CO₂ electroreduction in aqueous electrolytes [1, 18, 41].

In organic electrolytes, increasing CO₂ solubility is accompanied by low electrolyte conductivity. While the volatilization of a large number of organic solvents causes environmental issues, Thus, organic solvent systems are typically applied in homogeneous catalysis or the design of mixed electrolyte systems [1, 18].

Ionic liquids consisting of cations and anions have been accepted as a potential new class of environmentally benign solvents. Because of their special features, such as near-zero vapor pressure, high electrical conductivity, high electrical and thermal stability, and high gas solubility, have attracted much interest. Their negligible vapor pressure, high ionic conductivity, and wide electrochemical windows, especially, make them outstanding alternatives to conventional electrolytes in electrochemical applications. Besides, ionic liquids show excellent activity in the CO₂RR, and also provide a medium for CO₂RR, and their strong absorption capacity for CO₂ effectively promotes CO₂RR. Moreover, the selectivity of CO₂RR can be greatly enhanced, and when ionic liquid is present, the hydrogen evolution reaction (HER) is suppressed. Despite recent significant progress in CO₂RR in ionic liquid-based

electrolytes, ionic liquids have drawbacks such as high cost, high viscosity, and the absence of hydrocarbons and alcohols [1, 18].

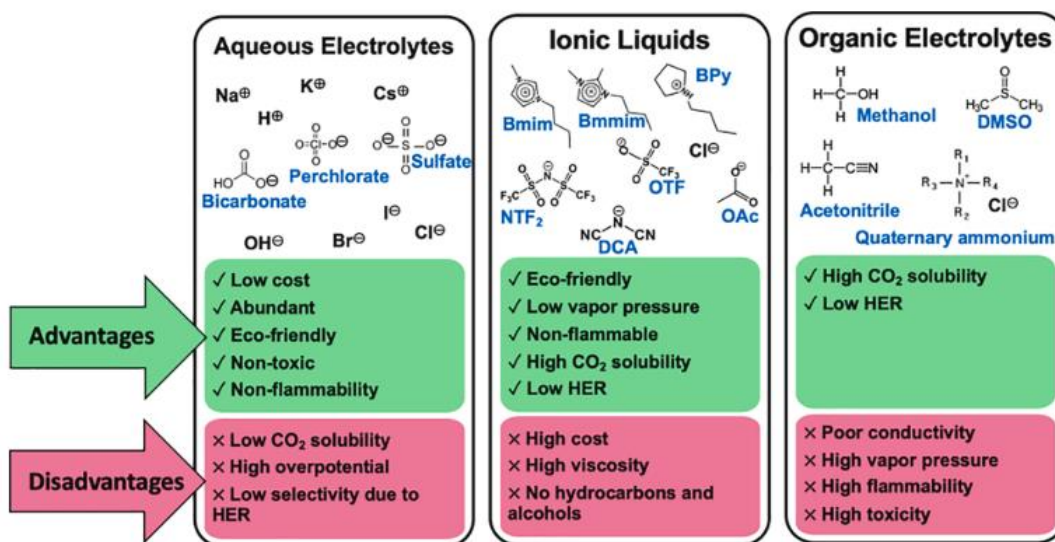


Figure 6. Compare electrolytes in CO₂RR [18]

From the ionic liquid structure as illustrated in Figure 7, the ionic liquid can be divided into two parts: the anion and the cation [18]. Imidazolium cations have been identified as specific promoters for CO₂RR that can reduce the overpotential for the reduction reaction due to their assistance in CO₂^{*} stabilization, inhibition of oxalate production, favoring CO and decreasing the overpotential [2, 16].

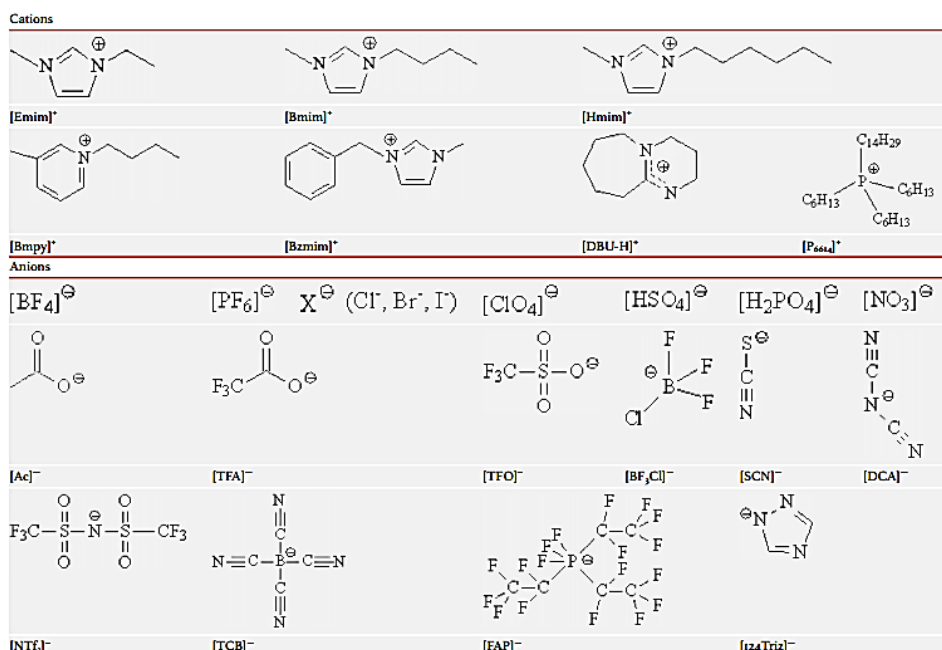


Figure 7. The structure of the ionic liquid [1]

The mechanism of ionic liquid in CO₂RR to any product depends on the type of ionic liquid, electrode, electrocatalysts, and overpotential [2]. Figure 8 shows one of the gas products mechanism as CO [42].

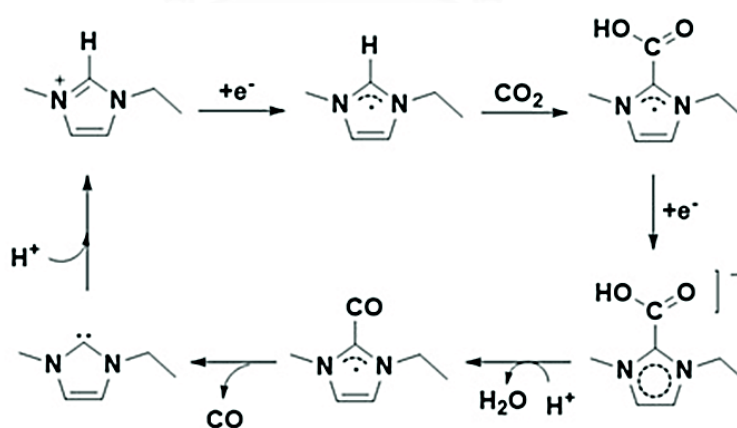


Figure 8. The mechanism of ionic liquid in CO₂RR to CO [42]

The mechanism of ionic liquid in CO₂RR to carbon product is shown in figure 9 and equations (1) - (8). When C_{ads} is carbon allotropes in the consecutive reaction steps for CO₂RR to C and the electrocrystallization that shown in as follows [16]:

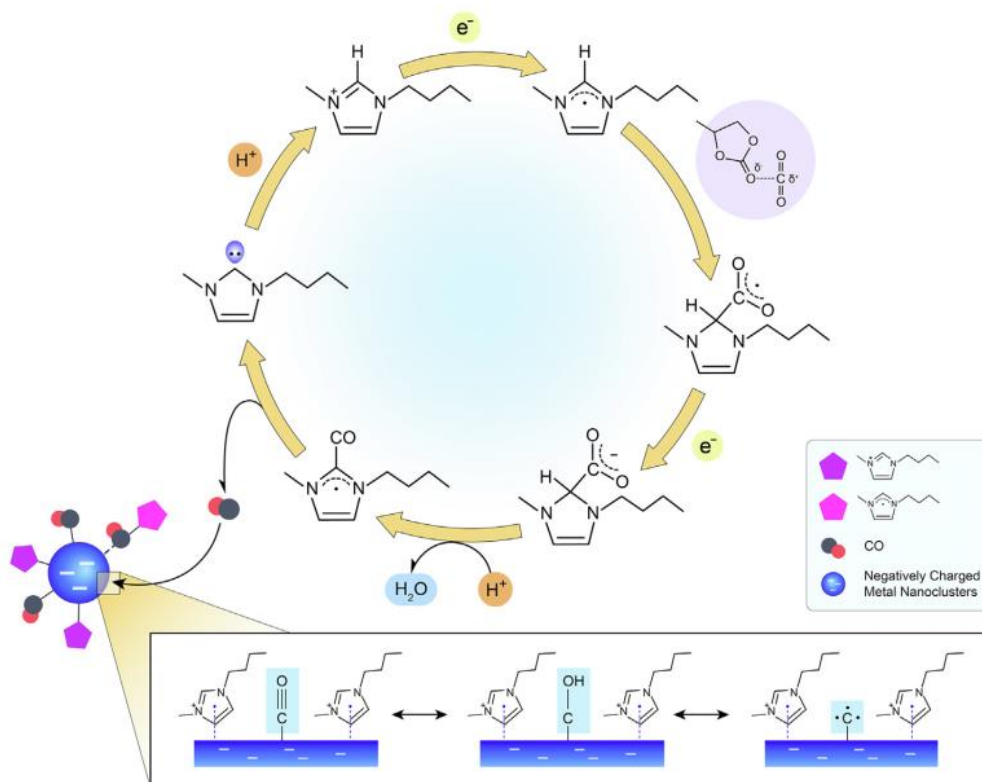
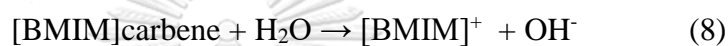
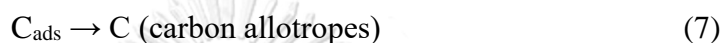
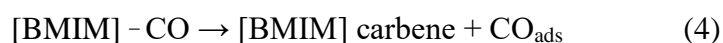
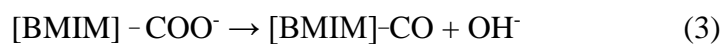
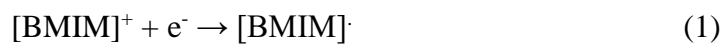


Figure 9. The mechanism of ionic liquid in CO₂RR to carbon product [16]

Table 2. Noble metal in CO₂RR

Electrode	Electrolyte	Potential (V)	Faradaic efficiency	Reference
Ag	0.1 M [P ₆₆₆₁₄] 124Triz/acetonitrile	-0.7 V vs. Ag/AgNO ₃	HCOO ⁻ = 63 %	Hollingsworth et al. 2015 [43]
Ag	[BMIM]BF ₄ /20% H ₂ O	-1.6 V vs. Ag/AgCl	CO >94 %	Rudnev et al. 2019 [44]
Ag	1 M ([EMIM]OH)Cl/ 2 M EG/PC	-1.7 V vs. Ag/AgCl	CO ~100 %	Vasilyev et al. 2019 [45]
Ag	0.1 M [BMIM]BF ₄ /PC	-1.9 V vs. Fc/Fc ⁺	CO = 98.5 %	Ju et al. 2020 [46]
Polycrystalline Ag electrode	8 mM [POHMIM][BF ₄] / 0.1 M TBABF ₄ /acetonitrile	-2.5 V vs. Fc/Fc ⁺	CO = 85 %	Zhang et al. 2017 [47]
Au	0.1 M [BMIM]BF ₄ / acetonitrile	-1.73 V to -1.93 V vs. NHE	CO = 95 %	Koh et al. 2015 [48]
Au(110)	[BMIM]BF ₄	-1.82 V vs. Ag/AgCl	CO = 95 %	Fu et al. 2018 [49]
Au	0.1 M [BMIM]OAc/ dimethylsulfoxide / 0.2 vol % H ₂ O	-1.80 V vs. Ag/AgCl	CO = 98 %	Gonçalves et al. 2019 [22]
Au foil	0.1 M [BMIM][Cl] / 0.1 M Bu ₄ NClO ₄ in PC	-2.5 V vs. Fc/Fc ⁺	CO ~90 %	Chen et al. 2018 [50]
Ag modified Cu	24 g [EMIM][BF ₄] + 1 g IL-Ag + CoCl ₂ (0.25 mg)	-2.0 V vs. SCE	CO >98 %	Zhou et al. 2015 [51]

The ionic liquid/PC mixture solution that was produced and considered as the electrolyte for CO₂RR on the Ag plate electrode was studied by Ju et al. 2020. In comparison to other ionic liquids investigated, found that the alkyl length of imidazole-based ionic liquids suggests that the [BMIM]BF₄ has a lower onset potential and Tafel slope, and also a larger exchange current density. The EIS results revealed that the imidazolium cation could absorb on the electrode surface and lower the overpotential by complexing with anion radicals (CO₂^{*-}) and stabilizing them. The values of the charge transfer resistances are arranged in order of [BMIM]BF₄/PC < [HMIM]BF₄/PC < [EMIM]BF₄/PC < [OMIM]BF₄/PC < [DMIM]BF₄/PC due to the

decrease in the chain length at the N1-position of the imidazolium cation from octyl to butyl, causing the catalytic activities of ionic liquid to increase. It can be concluded that the higher adsorbed quantity is caused by a lower steric hindrance of shorter chain length. Meanwhile, when the chain length decreases from butyl to ethyl, the adsorbed [Emim]⁺ increases, leading the film layer to become too thick to allow CO₂ molecules to pass through, which is undesirable for CO₂ conversion. Therefore, the [BMIM]BF₄ provides the highest performance for the conversion of CO₂. According to the performance tests, at 1.9 V (vs. Fc/Fc⁺), FE for CO can reach 98.5% and a current density of 8.2 mA/cm² can be achieved in [BMIM]BF₄/PC electrolyte solution [46].

Table 3. Post-transition metal in CO₂RR

Electrode	Electrolyte	Potential (V)	Faradaic efficiency	Reference
Bi	0.5 M KHCO ₃	-0.74 V vs. RHE	HCOO ⁻ ~89 %	Hyun Koh et al. 2017 [52]
Bi ₂ O ₂ CO ₃ @Bi/CP	0.5 M KHCO ₃	-1.07 V vs. RHE	HCOO ⁻ ~ 90 %	Liu et al. 2022 [25]
Sn/C-GDEs	0.45 M KHCO ₃ / 0.5 M KCl	-1.5 V vs. Ag/AgCl	HCOO ⁻ = 70 %	Castillo et al. 2017 [53]
Bi	100 mM [BMIM]OTF/ acetonitrile	-1.95 V vs. SCE	CO = 78 ± 5 %	Medina-Ramos et al. 2015 [54]
Sn		SCE	CO = 77 ± 5 %	
Pb		-2.05 V vs. SCE	CO = 81 ± 5 %	
Sn	[BMIM]BF ₄ / acetonitrile/water	-2.2 V vs. Ag/AgCl	HCOO ⁻ = 94.3 ± 2 %	Qinggong Zhu et al. 2016 [17]
Sn	0.5 M [EMIM]N(CN) ₂ /H ₂ O	-1.2 V vs. RHE	HCOO ⁻ = 81.9 %	Zhang et al. 2017 [55]
Pb	700 mM [BMIM] 124Trizu/acetonitrile/ 5 wt % H ₂ O	-2.4 V vs. Ag/AgCl	HCOO ⁻ = 95.2 %	Feng et al. 2018 [56]
MoO ₂ /Pb	0.3 M [BMIM]PF ₆ /acetonitrile	-2.60 vs. Fc/Fc ⁺	CO = 63.3%	Hu, Y.O.a.X. 2015 [20]
Pb phytate	12.8 wt % [BzMIM]BF ₄ /	-2.25 V vs.	HCOO ⁻ = 92.7 %	Wu et al.

	9.9 wt % H ₂ O /acetonitrile	Ag/AgCl		2018 [57]
In	Dimcarb	-1.34 V vs. Cc/Cc ⁺	CO = 45 % HCOO ⁻ = 40 %	Chen et al. 2016 [58]
In	[BMIM]PF ₆ /acetonitrile/ 1 mM In(acac) ₃	-1.9 V vs. SCE	CO = 99 %	Ding et al. 2016 [59]

The outcome of CO₂RR between noble metals and post-transition demonstrated that post-transition metals may perform as well as noble metals. Since the post-transition metal is more common, affordable, and nontoxic than the noble metal, it is interesting for use and development in CO₂RR [1].

2.6 Bi electrocatalysts

Bismuth (Bi) is an interesting material used in the development of heterogeneous CO₂ reduction catalysts because it is non-toxic and has a low environmental effect. Besides, Bi is a byproduct of the refining of Pb, Cu, and Sn and has few significant commercial applications, leading to its low and stable price. The development of Bi-based cathodes for CO₂RR would be an important development for the fields of CO₂ electrocatalysis and renewable energy conversion [4].

Table 4. Bi electrocatalyst in the CO₂RR

Electrode	Electrolyte	Potential (V)	Faradaic efficiency	Reference
Bi/C	0.5 M KHCO ₃	-1.6 V vs. Ag/AgCl	HCOO ⁻ = 93 ± 2.5%	Ávila-Bolívar et al. 2019 [10]
Bi-Sn/Cu	0.1 M KHCO ₃	- 1.0 V vs. RHE	HCOO ⁻ = 94.8%	Zong Li et al. 2022 [15]
Bi-CMEC	20 mM [BMIM]BF ₄ / acetonitrile/0.1 M TBAPF ₆	-1.95 V vs. SCE	CO = 95 ± 6 %	DiMeglio et al. 2013 [4]
Bi-CMEC	300 mM [BMIM]OTF/ acetonitrile	-2.0 V vs. SCE	CO = 87 ± 8 %	Medina-Ramos et al. 2014 [5]
Bi-CMEC	250 mM [BMIM]PF ₆ / acetonitrile/0.1 M	-1.95 V vs. SCE	HCOO ⁻ = 10 ± 2 % CO = 84 ± 3 %	Atifi et al. 2018 [11]

	TBAPF ₆			
	250 mM [DBU-H]PF ₆ /		HCOO ⁻ = 77 ± 5 %	
	acetonitrile/0.1 M		CO = 21 ± 1 %	
	TBAPF ₆			
	0.1 M [BMIM]OTf/			
	acetonitrile/0.1 M		CO = 90 ± 3 %	
	TBAPF ₆			
Bi-CMEC	0.1 M [BMIM]OTf/	-2.05 V vs. SCE	CO = 81 ± 4 %	Atifi et al. 2019 [60]
	DMF/0.1 M TBAPF ₆			
	0.1 M [BMIM]OTf/		CO = 66 ± 6 %	
	DMSO/0.1 M TBAPF ₆			
	0.1 M [BMIM]OTf/		CO = 63 ± 6 %	
	PC/0.1 M TBAPF ₆			
Bi/C	0.1 M [BMIM][OTf] in	-2.0 V vs.	CO = 96.1 ± 0.7 %	Zhang et al.
	acetonitrile	Ag/AgCl		2016 [61]
Bi/Sn	[BMIM]PF ₆ /PC/H ₂ O	-1.1 V vs.	C = 1.035	Rungkiat et al.
	4:5:1 by volume	Ag/AgCl	mmole.cm ⁻² .min ⁻¹	2022 [16]
Mo-Bi	0.5 M [BMIM]BF ₄ /	-0.7 V vs.	CH ₃ OH = 71.2%	Xiaofu Sun et
BMC/CP	acetonitrile	SCE		al. 2016 [62]
Bi ₂₂ Sn ₅₀ Pb ₂₈	0.1 M [BMIM]OTf/	-1.95 V vs. SCE	CO = 85 ± 4 %	Kunene et al.2020 [63]
	acetonitrile/0.1 M TBAPF ₆			

DiMeglio et al. 2013 investigated the efficacy of a low-cost bismuth-carbon monoxide evolving catalyst (Bi-CMEC) in none ionic liquid, 1ethyl-3-methylimidazolium tetrafluoroborate ([EMIM]BF₄), the BF₄⁻ salts of 1-butyl-3-methylimidazolium ([BMIM] BF₄), and 1-butyl-2,3-dimethylimidazolium·BF₄ ([BMMIM]BF₄). According to the findings, it was found that Bi-CMEC can be formed upon the cathodic polarization of an inert glassy carbon electrode in acidic solutions containing Bi³⁺ ions. This catalyst can be employed in combination with ionic liquids to perform electrocatalytic CO₂ to CO conversion with a current density at overpotentials of less than 0.2 V. Bi-CMEC is selective for CO generation with approximately 95% Faradaic efficiency, which is a high-energy efficiency for CO production comparable to that previously only seen with pricey silver and gold cathodes. CO₂RR's performance result is none ionic liquid < ([EMIM]BF₄) <

([BMMIM]BF₄) < ([BMIM] BF₄) for three reasons: the ionic liquid in CO₂RR is found critical to the electrocatalysis, and then deprotonation of the central imidazolium carbon of the [EMIM] and [BMIM], which is the main source of protons to operate the 2e⁻/2H⁺ conversion of CO₂ to CO. And since the proton transfer from the imidazolium helps drive the CO₂RR, the [BMMIM]BF₄, which carries a methyl substituent at the imidazolium 2-position, is unable to be deprotonated as readily so it does not induce CO₂RR catalysis. This implies that other organic acids could be capable of promoting similar electrocatalysis [4].

The Bi-CMEC performance in different catholyte anions of [BMIM], including potentially corrosive anions such as chloride and bromide, was studied by Medina-Ramos et al. 2014. It was found that the material could act as a strong carbon monoxide evolution catalyst and promote the electrocatalytic reduction of CO₂ to CO in the presence of suitable imidazolium ionic liquid promoters. Furthermore, it demonstrated that it can catalyze CO evolution with current densities up to $j_{CO} = 25\text{--}30 \text{ mA/cm}^2$ and associated energy efficiencies of $\Phi_{CO} \approx 80\%$ for the cathodic half-reaction. Regarding the anion effect, it was found that Cl^- , $\text{Br}^- < \text{BF}_4^-$, $\text{PF}_6^- < \text{OTf}^-$ since [BMIM]Br and [BMIM]Cl were more hygroscopic than the other anions studied, due to the presence of water in the electrolyte solution which may lead to the formation of other CO₂ reduction products like forms. These metrics emphasize the efficiency of Bi-CMEC, as it was previously shown that only noble metals promote fuel forming half-reaction with such high energy efficiency. Additionally, at an applied overpotential of $\eta \approx 250 \text{ mV}$ for a cathode with a surface area of 1.0 cm^2 , the rate of CO production by Bi-CMEC varies from around $0.1\text{--}0.5 \text{ mmol}\cdot\text{cm}^{-2}\cdot\text{h}^{-1}$, indicating that the concentration of Bi electrocatalysts does not influence the overpotential [5].

Xiaofu Sun et al. 2016 researched CO₂RR to methanol in [BMIM] BF₄/ MeCN using a Mo-Bi bimetallic chalcogenide (BMC) as an electrocatalyst on carbon paper (CP) as an electrode because the efficiency and selectivity of methanol in CO₂RR in the ionic liquid are currently low. The results revealed that Mo-Bi BMC/CP with a Mo: Bi molar ratio of 1:1 was a very efficient and stable electrode for electrochemical

CO₂ to methanol reduction. For CO₂ electrochemical reduction to methanol, the Faradaic efficiency can be as high as 71.2% with a current density of 12.1 mA.cm⁻² when using 0.5 M [BMIM]BF₄ in MeCN as the electrolyte, which is substantially higher than the values reported thus far. The synergistic effect of Mo and Bi in CO₂RR caused the high electrocatalytic selectivity of the Mo-Bi BMC/CP electrode for methanol production. Bi increases the conversion of CO₂ to CO, and Mo prefers the generation of H₂ and can bind CO. Consequently, the CO is bonded and can be further hydrogenated to get methanol. It could follow with the pathway of CO₂ → CO₂^{*-} → CO_{ads} → CHO_{ads} → CH₃O_{ads} → methanol. This research suggests a new and effective way of producing methanol from CO₂ in [BMIM] BF₄/ MeCN. The electrode comparison between Mo-Bi BMC/CP, Mo-Ag BMC/CP, and Mo-Cu BMC/CP showed that the competitive hydrogen-evolution reaction (HER) is poor at low potential (Mo-Bi BMC/CP < Mo-Ag BMC/CP < Mo-Cu BMC/CP) and CO₂ reduction tends to occur with the increased potential. Methanol had its highest Faradaic efficiency at -0.7 V (vs. SHE), while the Mo-Bi BMC/CP efficiency was better than the Mo-Ag BMC/CP and Mo-Cu BMC/CP electrodes due to the ability of Bi sites to stabilize CO₂^{*-} intermediates in the presence of ionic liquid [62].

The efficient electrochemical conversion of CO₂ to CO on surface-activated bismuth nanoparticles (NPs) in acetonitrile (MeCN) at ambient conditions with [BMIM][OTf] was studied by Zhang et al. 2016. By comparing electrodeposited Bi films (Bi-ED) and different types of Bi NPs, it was demonstrated for the first time the effect of catalyst size and surface condition on organic electrochemical CO₂ reduction. The result showed that the surface inhibiting layer (hydrophobic surfactants and Bi³⁺ species) formed during the synthesis and purification process hinders the CO₂ reduction, resulting in a 20% decrease in Faradaic efficiency for CO evolution (FE_{CO}). When the surface of Bi was air-oxidized, the Bi particle size had a significant effect on FE_{CO}, whereas this size dependence of FE_{CO} became negligible on surface-activated Bi NPs. After the surface activation (hydrazine treatment) that effectively removed the native inhibiting layer, at -2.0 V (vs. Ag/AgCl), activated 36 nm Bi NPs showed quantitative conversion of CO₂ to CO (96.1% FE_{CO}) and a mass activity for

CO evolution (MA_{CO}) of 15.6 mA mg^{-1} , three times greater than the typical Bi-ED. This research highlights the importance of surface-activation for efficient electrochemical CO_2 conversion on metal NPs and leads to a better understanding of the CO_2 electrochemical reduction mechanism of CO_2 in non-aqueous media [61].

Atifi et al. (2019) studied the improvement of catholyte solvent in CO_2RR by using Bi-CMEC. The catholyte solvents were tested including acetonitrile (MeCN), N, N-dimethylformamide (DMF), dimethyl sulfoxide (DMSO), and propylene carbonate (PC). The result showed that controlled potential electrolysis (CPE) current is highly dependent upon the solvent choice, increasing in the order $PC < DMSO < DMF < MeCN$. CPE showed that the rate and selectivity of this process are strongly dependent on solvent choice. In surveying a series of polar aprotic catholyte solvents, it was found that although MeCN and DMF-based catholyte give rise to rapid and selective CO evolution, the use of DMSO or PC leads to much lower j_{CO} (i.e., slower kinetics) and FE_{CO} (i.e., reduced selectivity) for the Bi/[BMIM]⁺ system. Analysis of the steady-state current density (j_{ss}) as measured by chronoamperometry and the efficiency for CO production (FE_{CO}) showed that both these metrics can be correlated with the ability of CO_2 to diffuse to the electrode surface. Upon accounting for the differing solubilities of CO_2 in the different solvents studied, it is clear that both j_{ss} and FE_{CO} are inversely related to the viscosity of the catholyte solvent. This dependency is to be expected since CO_2 is the substrate for electrocatalysis and the rate-limiting step of CO generation involves electron transfer to CO_2 at the Bi cathode. Other unexpected findings concerning the role of the imidazolium in the Bi/[BMIM]⁺ system were also discovered. In addition to the catalytic production of CO being dependent on the mass transport of CO_2 to the cathode surface, the ability of the [Im]⁺ to diffuse to the Bi cathode is strongly correlated with the efficacy of the electrocatalytic reduction. Moreover, the ability of [Im]⁺ to access the Bi/catholyte interface not only strongly influences the rate at which CO is produced by the Bi electrocatalyst, but also is well correlated with the selectivity displayed for CO generation in each of the electrolyte solvents surveyed. It is recognized that the accumulation of [Im]⁺ at the Bi cathode is critical to the rapid conversion of CO_2 to

CO, giving motivation for studies about CO₂ electrolysis using the Bi film electrode in neat imidazolium-based ionic liquids, which ensure that large concentrations of [Im]⁺ are maintained at the cathode during catalysis. These experiments revealed that they were highly selective [60].

Kunene et al. 2020 studied the ability of the inexpensive commercially available alloy of Bi, Sn, and Pb, which is known as Rose's Metal (RM) to drive the electrocatalytic reduction of CO₂ to CO within the presence of [BMIM]OTf in MeCN-based electrolytes. The result showed that these substrates had a surface composition (Bi₂₂Sn₆₀Pb₁₈) that was enriched in Sn relative to the other two post-transition metal elements. Voltammetric and electrolysis experiments demonstrate that the RM/[BMIM]⁺ catalyst interface is a selective (FE_{CO} = 80–95%) and robust platform for CO evolution and operates with modest activity ($j_{\text{tot}} = 3\text{--}10 \text{ mA/cm}^2$) at potentials more negative than -1.80 V vs. SCE in MeCN. Accordingly, the RM/[BMIM]⁺ platform is predominately a CO evolving catalyst system much like the electrodeposited monometallic Bi, Sn, and Pb thin films that were also studied [63].

Rungkiat et al. 2022 studied a novel approach to obtain nanocrystalline carbon products using the room temperature CO₂RR on various particulate metal electrocatalysts such as Bi, Ag, Co, and Zn at a low applied potential of -1.1 to $-1.6 \text{ V vs. Ag/AgCl}$ under the ternary electrolyte system containing [BMIM] BF₄, propylene carbonate (PC), and water at room temperature. Without any liquid products, the outcome of the nanocrystalline carbon was formed as the main product from CO₂ (selectivity of approximately 96% or above, $\sim 1 \text{ nm}$ thickness). When a negative potential was applied, nanoclustering of the self-limiting ultrathin metal oxide layers of metal particles on the highly conductive substrate could cause the formation of negatively charged metal clusters, which were efficiently sustained by the ternary electrolyte system. This system enables CO₂ to be reduced to single atoms C* and the subsequent electrocrystallization of C* into carbon allotropes on the crystallographic planes of the single crystal metals formed as the building blocks. The CO₂-derived Ag-C/epoxy composites reveal promising thermal conductivity. The results propose

the development of the growth of nanostructured carbon allotropes from CO₂ by the viable negative CO₂ emission approach [16].



CHAPTER III

MATERIALS AND METHODS

This chapter explains the experimental procedure, including the materials, catalyst preparations, characterization techniques, and experimental setup for CO₂RR.

3.1 Materials

Table 5. The materials and chemicals used in the electrodeposition method.

Chemicals/Materials	Formula	Suppliers
Bismuth(III) nitrate pentahydrate	Bi(NO ₃) ₃ · 5H ₂ O	Sigma-Aldrich
Nitric acid	HNO ₃	Emsure
Platinum rod (Length 76 mm, Diameter 2 mm)	Pt	Metrohm
Tin foil (0.1 mm thick, 99.998%)	Sn	Alfa Aesar

Table 6. The materials and chemicals used in the CO₂RR.

Chemicals/Materials	Formula	Suppliers
Platinum foil (0.1 mm thick, 99.9999%)	Pt	Alfa Aesar
Potassium hydrogen carbonate	KHCO ₃	Acros Organics
1-Butyl-3- methylimidazolium tetrafluoroborate	[BMIM]BF ₄	Sigma-Aldrich
Propylene carbonate	PC	Sigma-Aldrich
High purity carbon dioxide	CO ₂	Lindre
High purity nitrogen	N ₂	Lindre

3.2 Catalysts preparation

3.2.1 Preparation of Sn electrode

Sn foil ($10 \times 25 \text{ mm}^2$) was mechanically polished with 800 G sandpaper and was measured Sn foil ($10 \times 10 \text{ mm}^2$). Next, the Sn electrode was cleaned with DI and dried at room temperature. After that, the working area on the Sn foil ($10 \times 10 \text{ mm}^2$) was prepared using pipe thread tape.

3.2.2 Preparation of Bi/Sn electrode

Bi/Sn electrode was prepared by the electrodeposition method. For Bi catalyst preparation, Bismuth nitrate pentahydrate, $\text{Bi}(\text{NO}_3)_3 \cdot 5\text{H}_2\text{O}$, was dissolved in 1 M HNO_3 to obtain the concentration of 0.01, 0.03, 0.05, 0.07, and 0.1 M. Then, the Bi catalysts were deposited on Sn foil ($10 \times 10 \text{ mm}^2$) in a two-electrode system containing Pt rod as an anode and Sn electrode as a cathode at the potential of -0.7 volt for 600 seconds. The experimental apparatus is shown in Figure 10. After that, the electrode was washed with DI and dried for 60 minutes at room temperature. The catalyst samples were named as 0.01Bi/Sn, 0.03Bi/Sn, 0.05Bi/Sn, 0.07Bi/Sn, and 0.1Bi/Sn electrodes.

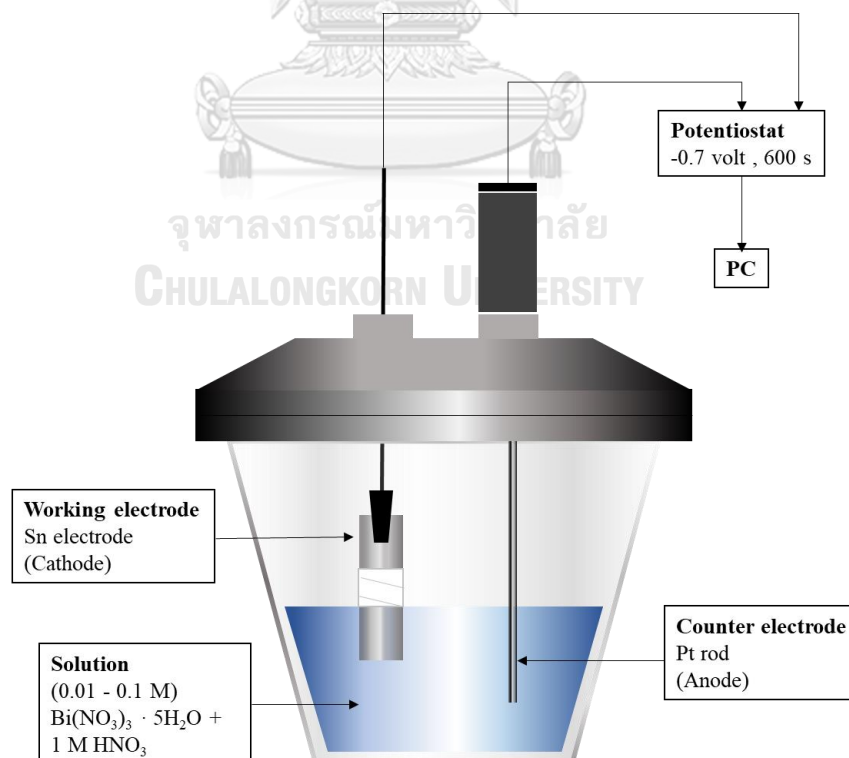


Figure 10. Electrodeposition of Bi catalysts on Sn electrode

3.3 Catalyst Characterization

0.01Bi/Sn, 0.03Bi/Sn, 0.05Bi/Sn, 0.07Bi/Sn, and 0.1Bi/Sn electrodes were characterized by scanning electron microscopy (SEM) of Hitachi mode S-3400N, energy dispersive X-ray spectroscopy (EDX), and X-ray photoelectron spectroscopy (XPS) to investigate the morphology, the electrode composition, and the surface chemical states of the electrocatalysts of the electrode surface, respectively.

3.4 H-type cell preparation

The H-type cell was prepared in the form of a three-electrode cell, as shown in Figure 11, and was used in all experiments at room temperature and ambient pressure. The Nafion® 117 membrane separated between a cathodic chamber and an anodic chamber. Two silicone gaskets were used to prevent liquid leakage between cells, and two sides of cells were combined using a clamp. The anodic chamber consisted of Pt foil as the counter electrode and 20 mL of 0.1 M KHCO_3 as electrolyte. The cathodic chamber consisted of the 0.01Bi/Sn, 0.03Bi/Sn, 0.05Bi/Sn, 0.07Bi/Sn, or 0.1Bi/Sn electrodes as a working electrode, Silver/Silver Chloride (Ag/AgCl) as the reference electrode, and the mixture of [BMIM]BF₄/PC/DI as electrolyte. [BMIM]BF₄/PC/DI ratio for all experiments was 55.2: 36.8: 8 %v/v. The silicone corks were used to prevent a gas leak in the system.

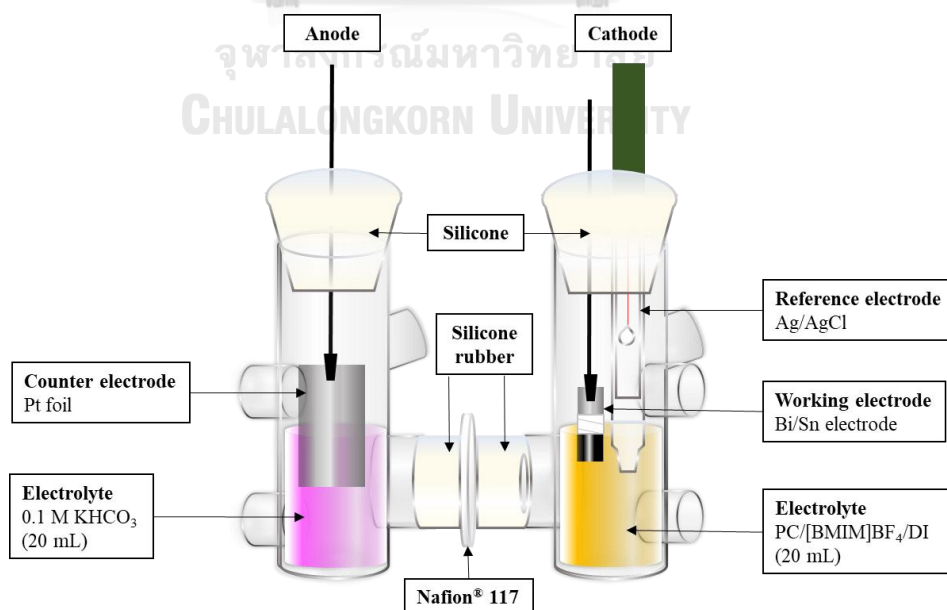


Figure 11. H-type cell preparation

3.5 Effect of Bi concentration on the properties of electrocatalyst

3.5.1 Linear sweep voltammetry (LSV)

Linear sweep voltammetry (LSV) is a simple method in electrochemical to find onset potential by a single linear sweep from the lower potential limit to the upper potential limit. In addition, it can be used to calculate the peak current, calculate the peak current potential, and calculate the half-peak current potential. However, it is suitable for irreversible systems where a reverse sweep would not reveal any more information in the reaction [64]. So, LSV was a method to find onset potential in CO₂RR. After setting up an H-type cell, the Nitrogen gas (N₂) flow rate of 100 mL/min was fed into the system for 60 minutes, and then a potentiostat ran the LSV program and showed the result on a personal computer (PC). Next, the CO₂ was fed into the system at 100 mL/min flow rate for 60 minutes. The working electrodes were 0.01Bi/Sn, 0.05Bi/Sn, or 0.1Bi/Sn electrodes. Afterward, The LSV results between N₂ and CO₂ were compared and found the onset potential for each Bi concentration.

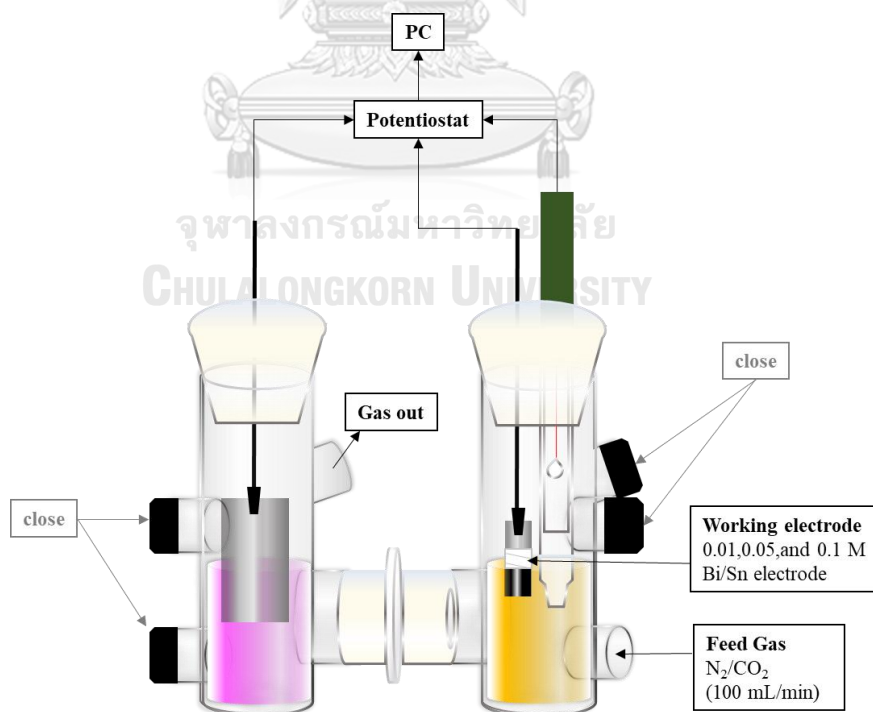


Figure 12. LSV experiment

3.5.2 Electrochemical Impedance Spectroscopy (EIS)

Electrochemical Impedance Spectroscopy (EIS) is a method to find impedance and electrical circuits in this system [65]. The H-type cell was set up. The CO₂ flow rate of 100 mL/min was fed into this system for around 60 minutes. Then, the EIS program in potentiostat ran at -1.1, -1.3, -1.5, and -1.7 V and showed the result on a personal computer (PC). The working electrodes were 0.01Bi/Sn, 0.05Bi/Sn, and 0.1Bi/Sn electrodes. lastly, The EIS results were compared and analyzed for each Bi concentration.

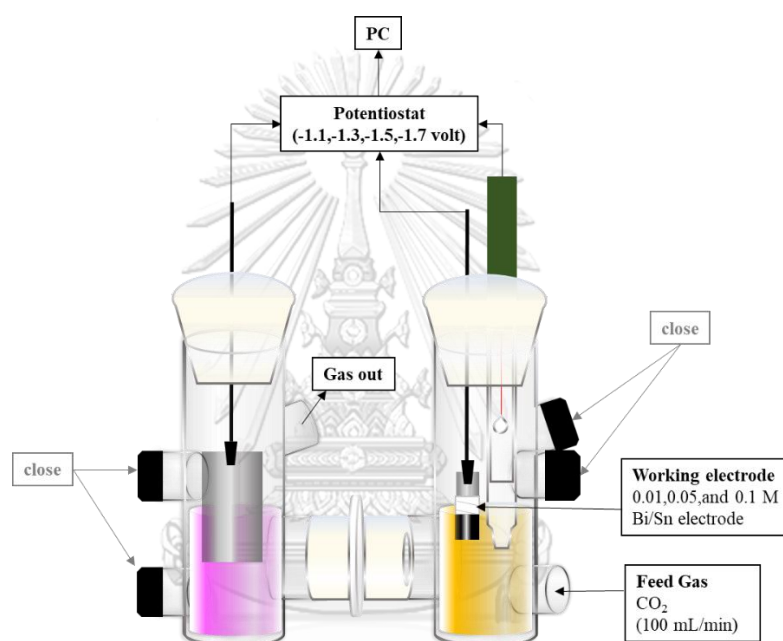


Figure 13. EIS experiment

3.5.3 CO₂RR performance

CO₂RR was a method to find the product in this system. The H-type cell was set up. The CO₂ flow rate of 100 mL/min was fed into this system for saturation around 60 min. Then, The CO₂ flow rate of 20 mL/min was fed during the running reaction. CO₂RR was run at -1.1 V vs. Ag/AgCl for 70 min by a potentiostat. The working electrodes were 0.01Bi/Sn, 0.03Bi/Sn, 0.05Bi/Sn, 0.07Bi/Sn, and 0.1Bi/Sn electrodes. The gas product such as CO and H₂ were detected by GC at the operating condition as shown in table 7. The liquid products were analyzed by using NMR and the solid product was detected by Raman spectroscopy. Moreover, it was characterized by SEM-EDX to investigate the morphology of the electrode surface and the electrode

composition and TEM-EDX-SAED (Transmission Electron Microscopy, Energy-dispersive X-ray spectroscopy, and Selected Area Electron Diffraction) of JEOL (JEM-2010) to study a morphologic analysis, structural and chemical of solid samples of the electrode at an atomic level.

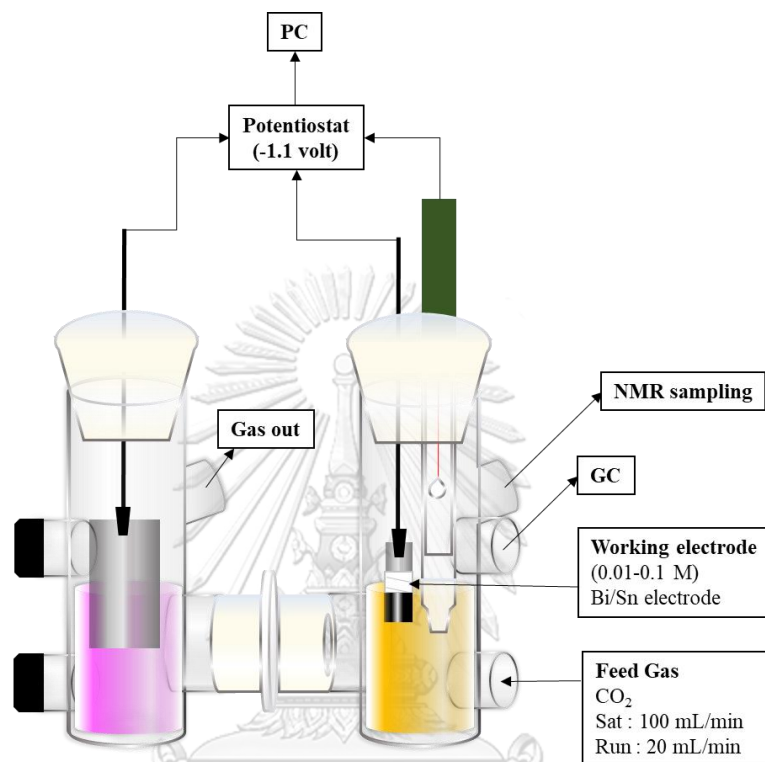


Figure 14. CO₂RR performance at -1.1 volt

Table 7. The operating conditions of GC

Gas chromatography (Shimadzu GC-2014)	Conditions
Detector	TCD
Column information	Shincarbon ST (50/80)
Carrier gas	Helium (99.999%)
Injector temperature	180°C
Column initial temperature	40°C, Hold time 5 min
Column temperature rate	10°C/min
Column final temperature	200°C
Detector temperature	170°C
Total time analysis	21 min

3.5.4 Result Analysis

From 3.5.1 to 3.5.3, The best Bi concentration was selected to study the CO₂RR performances and characterization of the Bi/Sn electrode.

3.6 Effect of potentials on electrocatalytic performance

The H-type cell was set up. The CO₂ flow rate of 100 mL/min was fed into this system for saturation proximately 60 min. Then, The CO₂ flow rate of 20 mL/min was fed during the running reaction. CO₂RR was run at -1.1, -1.3, -1.5, and -1.7 V vs. Ag/AgCl for 70 min by a potentiostat. The working electrode was Bi/Sn electrodes by using the best Bi concentration. Moreover, It was characterized by SEM-EDX to investigate the morphology of the electrode surface and the electrode composition. The gas product such as CO and H₂ were detected by GC. The liquid products were analyzed by using NMR and the solid product was detected by Raman spectroscopy.

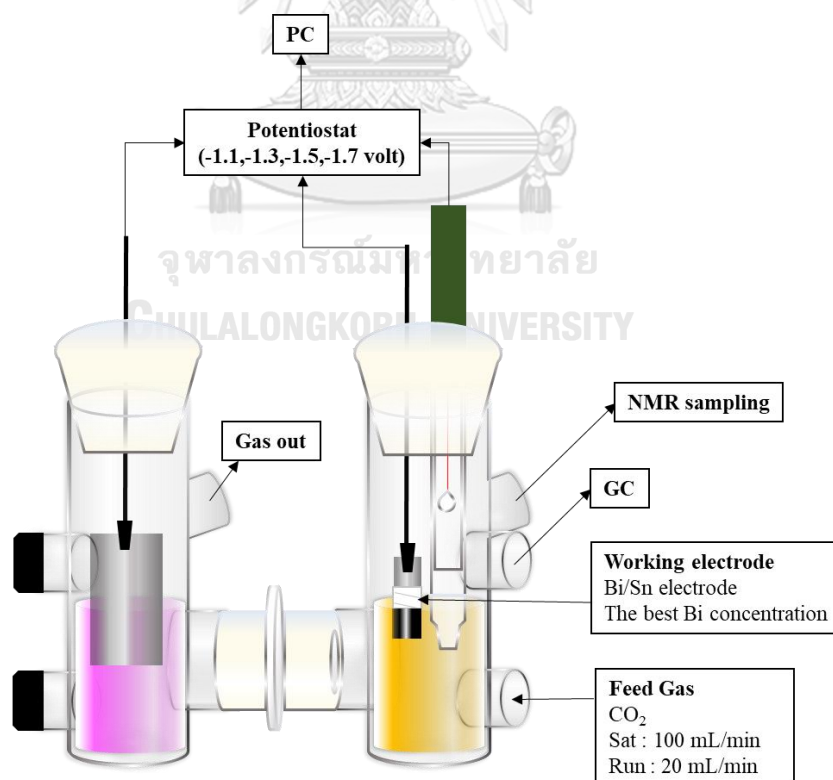


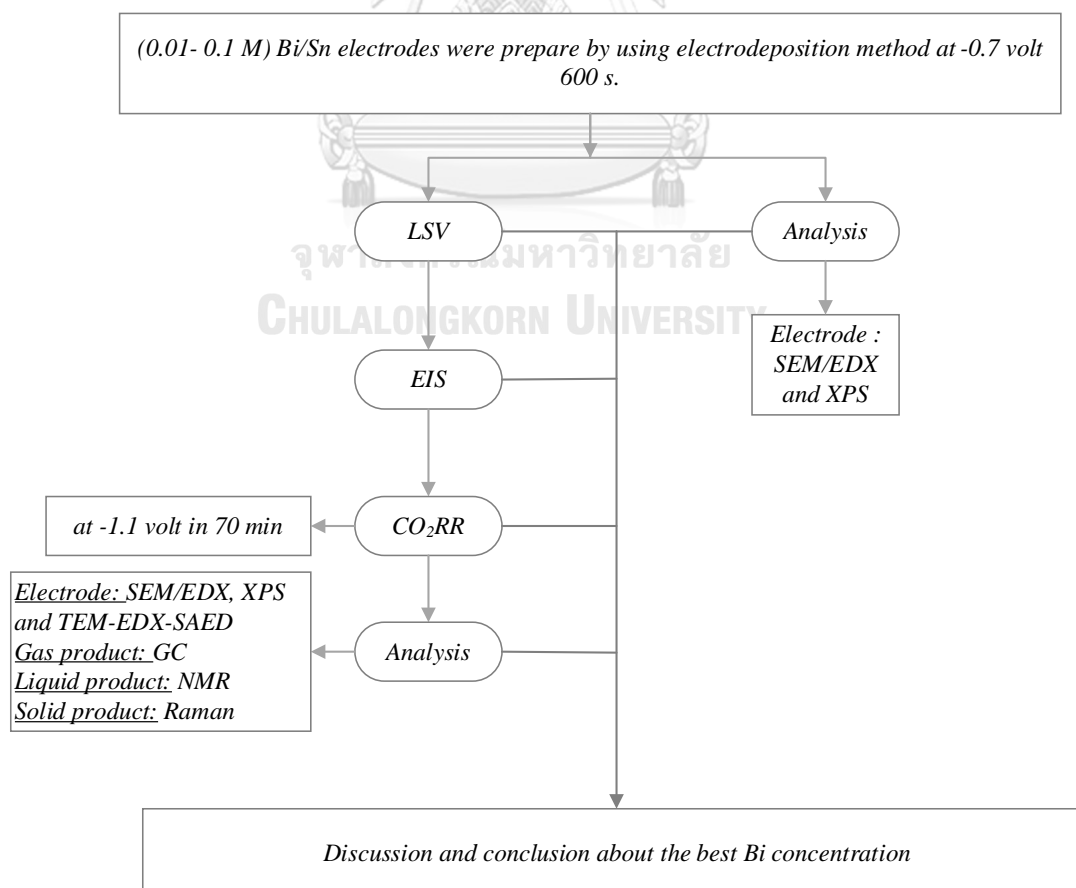
Figure 15. CO₂RR performance by varied potentials

3.7 Stability test of electrocatalyst

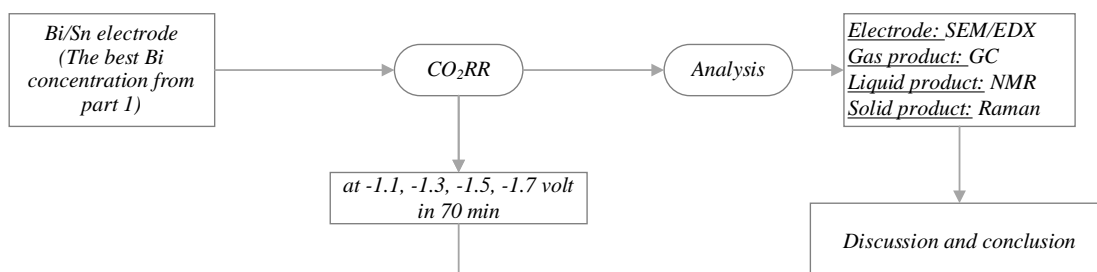
The H-type cell was set up. The CO₂ flow rate of 100 mL/min was fed into this system for saturation proximately 60 min. Then, The CO₂ flow rate of 20 mL/min was fed during the running reaction in 70 min compared with 150 min. CO₂RR was run at the best of potential from the study of the effect of potential. Moreover, It was characterized by SEM-EDX to investigate the morphology of the electrode surface and the electrode composition. The gas product such as CO and H₂ were detected by GC and for 150 min Condition, the GC kept a sample every 30 min. The liquid products were analyzed by using NMR, and the solid product was detected by Raman spectroscopy.

3.8 Research methodology

3.8.1 **Part 1:** To study the effects of Bi concentration on electrodeposition process, characteristic, and performance of Bi/Sn electrode for CO₂RR performance in [BMIM]BF₄/ PC/DI electrolyte.



3.7.2 **Part 2:** To study the suitable potential for the CO₂RR performance to produce carbon allotropes in [BMIM]BF₄/ PC/DI electrolyte.



CHAPTER IV

RESULTS AND DISCUSSIONS

This chapter explains the results and discussion from the experimental which are divided into two parts. Part 1 is for the study of effect of Bi concentration and Part 2 for the study of effect of applied potential on electrodeposition process, characteristic, and CO₂RR performance in [BMIM]BF₄/ PC/DI electrolyte.

4.1 Characterization of Bi/Sn electrode with various concentrations

4.1.1 SEM-EDX

4.1.1.1 SEM Characterization of Sn electrode

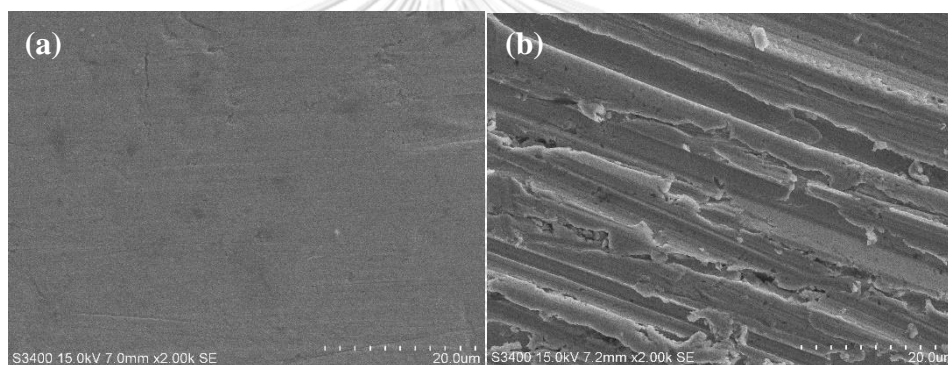


Figure 16. SEM images of Sn electrode: (a) Sn electrode (b) Sn electrode after mechanically polishing

The SEM results of the Sn foil in Figure 16 show the surface of Sn foils before and after mechanical polishing. As can be seen in these figures, mechanical polishing resulted in a rougher Sn electrode surface for increasing the surface area of the electrode surface in electrodeposition [66].

4.1.1.2 SEM-EDX Characterization of Bi/Sn electrode by electrodeposition

The SEM results of the Bi/Sn electrodes prepared by electrodeposition at -0.7 volt with 0.01 M – 0.1 M Bi concentrations are illustrated in Figure 17. The magnification of the left figure is 10 μ m, whereas the magnification of the right figure is 20 μ m for the same row coming from the same electrode.

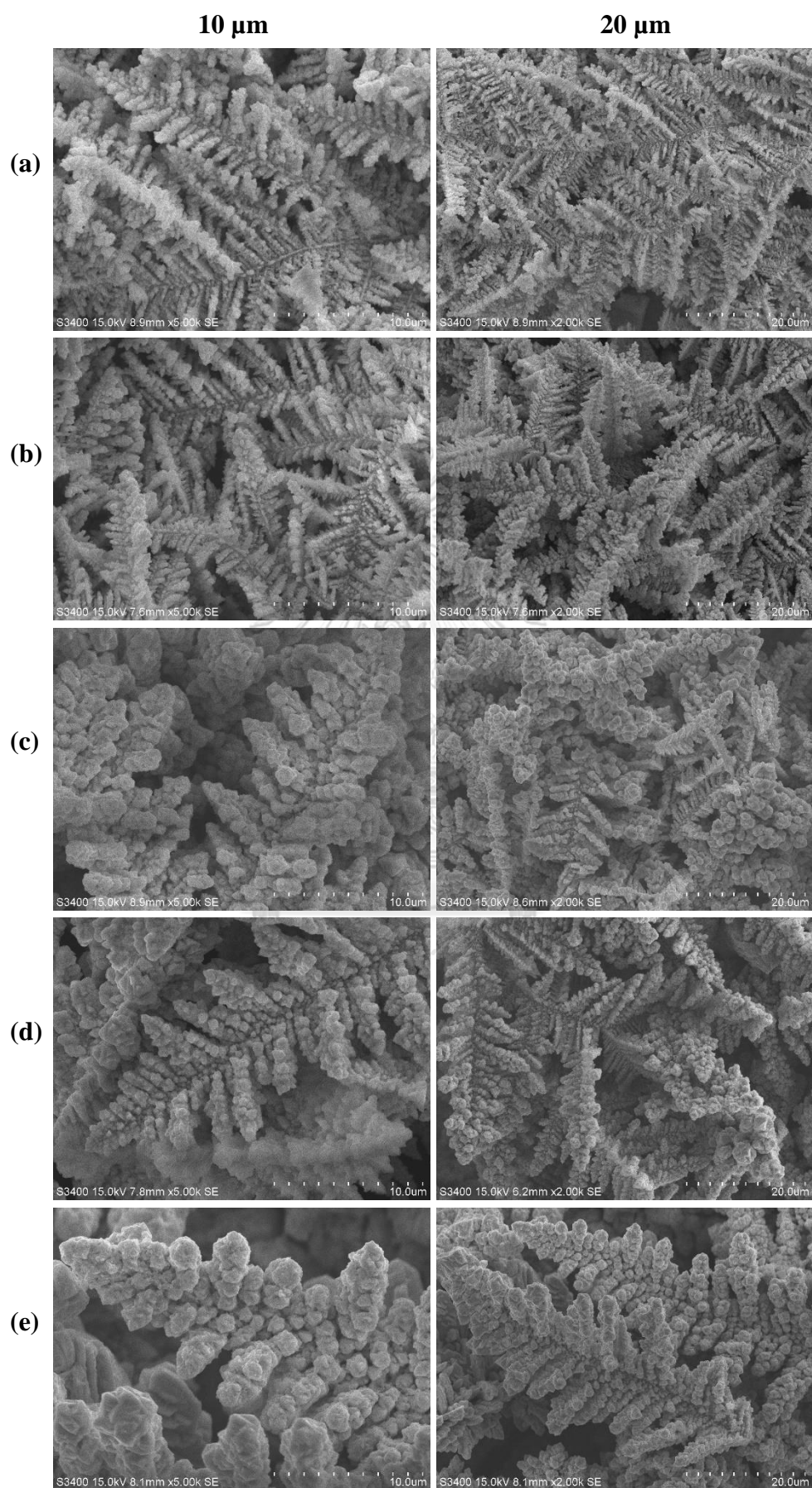


Figure 17. SEM images of Bi/Sn electrode : (a) 0.01 M (b) 0.03 M (c) 0.05 M (d) 0.07 M and (e) 0.1 M Bi/Sn electrode

The morphology of all Bi concentrations on the Sn electrode showed a dendrite structure, which is similar to the results of Rungkiat et al. 2022 [16]. The various magnifications represent dendrite sizes and distributions, respectively. At a magnification of 10 μm , concentration affects the size of dendrites by increasing dendrite size as concentration increases, similar to the results of Zhang et al. 2019 [67]. At a magnification of 20 μm , the image reveals distributions. On the surface of the electrode, numerous small dendrites were observed at low concentrations. When the concentration increases, the dendrites will group together and form larger and taller than the distribution on the electrode surface. The result corresponds to the EDX result in Table 8.

Table 8. EDX results of 0.01-0.1 M Bi on Sn electrode.

Catalyst	The percent by atom (%)		
	Bi (%)	Sn (%)	O (%)
0.01Bi/Sn	52.80	10.67	36.53
0.03Bi/Sn	43.54	13.26	43.20
0.05Bi/Sn	40.73	11.67	47.60
0.07Bi/Sn	37.60	13.50	48.89
0.1Bi/Sn	42.65	13.49	43.86

EDX was used to study the elemental distribution on the electrodes and the results are shown in Table 8. It was found that the electrode prepared with 0.01 M Bi concentration had the highest %Bi atom on a particular electrode surface, suggesting that they are densely distributed Bi at the specific surface. Increased Bi concentration, on the other hand, resulted in a lower percentage of Bi atoms on the surface. At a higher Bi concentration, the Bi particles may be more likely to deposit on the Bi particles than on the Sn substrate, resulting in larger Bi dendrites, as seen in the SEM images.

According to Grujicic et al.2002 [28], the Bi atoms in lower Bi concentrations were spaced further apart than in higher Bi concentrations. Atoms, once distributed on a particular surface in the atomic state, must move toward each other to minimize the surface energy. For atoms spaced by a large distance, instead of traveling a long distance to form dendrites, which is energetically unfavorable, they will group with their nearest neighbors, resulting in many small dendrites. In comparison, when the

initial number of reduced Bi atoms is large, the closeness of the atoms is grouped to form large and high dendrites to reduce energy. The size of each dendrite determines the size of its diffusion zone.

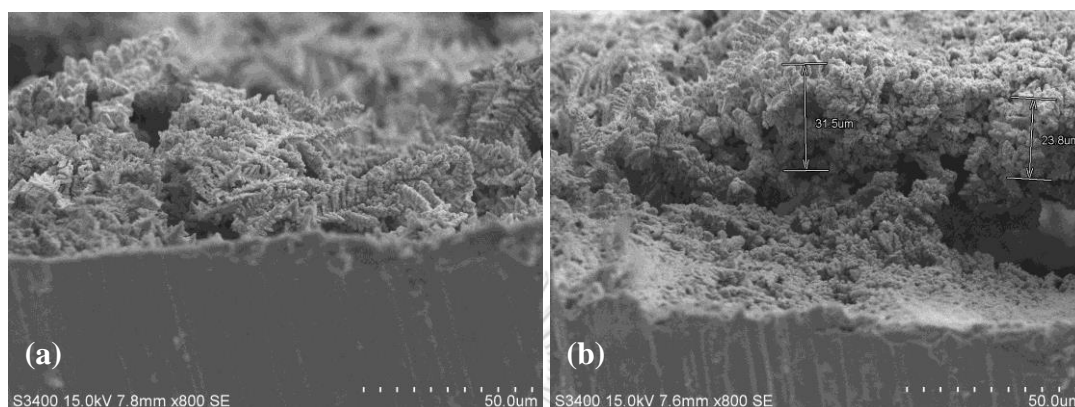


Figure 18. 0.05 M Bi/Sn electrode cross-section by SEM

When the concentration increases on the electrode surface, the dendrites will group together and form larger and taller than the distribution on the electrode surface is confirmed by the results of the 0.05 M Bi/Sn electrode cross-section in Figure 18. Figure 18 (a) shows the dendrite structure from Bi on the Sn electrode surface. In Figure 18 (b) shows the space between the group of Bi on the dendrite structure and Sn electrode surface and exhibits the thickness of 0.05 M Bi/Sn electrode around 30 μm [68, 69].

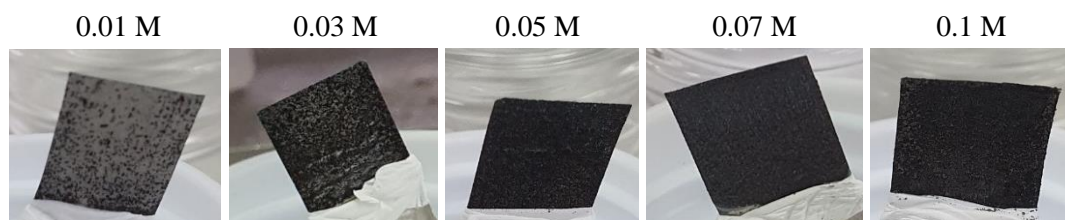


Figure 19. Bi/Sn electrodes prepared by electrodeposition of Bi^{3+} on Sn foil

Furthermore, as shown in Figure 19, 0.01 M and 0.03 M, it was found that Bi did not cover the whole electrode working areas. Also, the Bi deposits at 0.1 M were very thick, and it was easy for Bi particles to detach from the Sn substrate.

4.1.2 XPS Characterization of Bi/Sn electrode by electrodeposition

XPS characterization was used to investigate the surface chemical states of the electrocatalysts of the (0.01-0.1M) Bi/Sn electrode surface after electrodeposition. The XPS results are shown in Figure 20. Bi concentrations at 0.01-0.07 M were observed in two XPS spectra of the Bi 4f. The Bi 4f peaks around binding energy 159 eV and 164 eV represent Bi 4f_{7/2} and Bi 4f_{5/2} [70, 71], respectively. The results of Bi 4f_{7/2} and Bi 4f_{5/2} refer to Bi³⁺ species in Bi oxide [72]. The Bi³⁺ species can help as an electrocatalyst in this system for CO products [4]. The binding energy at 0.07 M shifts to lower, which means electrical conductivity on the electrocatalyst surface increased [73, 74]. At 0.1 M, The Bi 4f peaks around binding energy 160 eV and 165 eV, which refers to Bi⁵⁺ species in Bi oxide [75-77]. The Bi⁵⁺ species can narrow the band gap in the electrocatalyst structure so that it can block charge transfer in this system [77]. From the XPS result, the intensity of Bi oxide is high, so it confirms that the Bi/Sn electrode surface of metal Bi was easily oxidized [72].

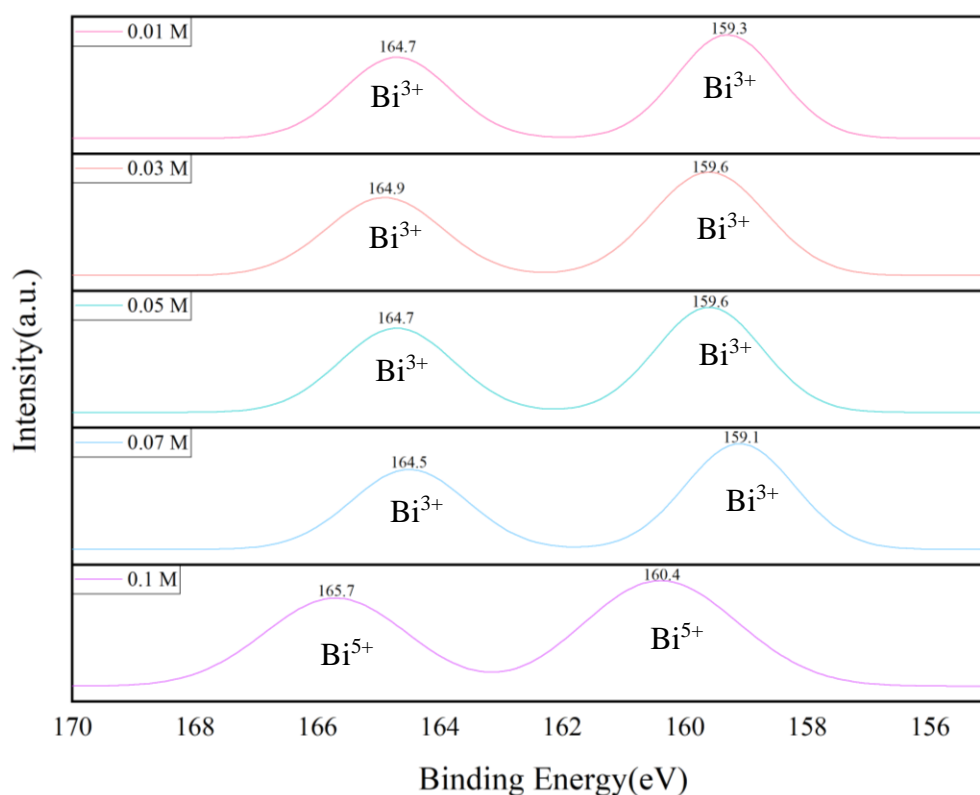


Figure 20. Bi 4f XPS spectra image of Bi/Sn electrode by electrodeposition

4.2 LSV of electrocatalysts prepared in various Bi concentrations bath

The onset potential of the CO₂RR of (0.01 M, 0.05 M, and 0.1 M) Bi on the Sn electrode in PC/BMIM[BF₄]/DI at the cathodic potentials of -0.7 V to -2 V vs. Ag/AgCl was studied using LSV experiments. Figure 21 exhibits the outcomes of LSV results in various gases. In the N₂ system, dashed lines showed the rate of hydrogen evolution reaction (HER), and in the CO₂ system, solid line showed the rate of the CO₂RR. The onset potential of (0.01 M, 0.05 M, and 0.1 M) Bi concentration was determined to be about -1.3 V to -1.4 V vs. Ag/AgCl. It indicates that Bi concentration range had no effect on the onset potential of the prepared Bi/Sn electrodes. Similar results were found by Medina-Ramos et al. [5].

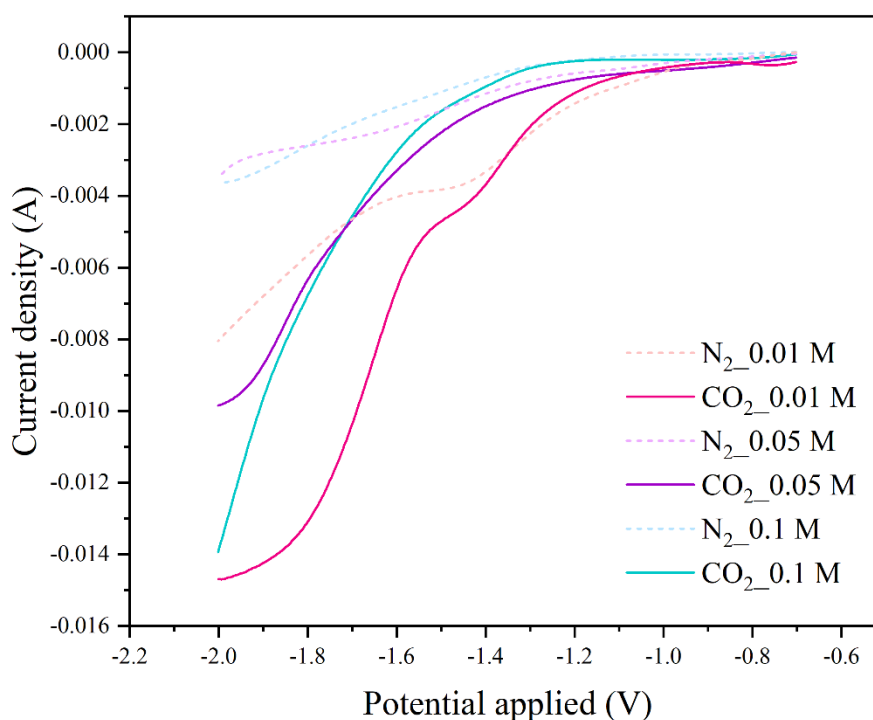


Figure 21. LSV result of Bi/Sn electrode

4.3 EIS with various Bi concentrations

The EIS was used to examine the charge transfer resistance (R_{CT}) at -1.1 V to -1.7 V during the CO₂RR by using (0.01 M, 0.05 M, and 0.1 M) Bi on the Sn electrode in PC/BMIM[BF₄]/DI. Figure 22 and Table 9 illustrate the results. In this experiment,

the EIS spectra obtained at -1.1 V and -1.7 V revealed the same trend. The R_{CT} was considerably reduced when 0.05 M Bi/Sn was used compared to other concentrations, which is believed to be due to an increase in the reactive area, including the edge site, by forming the porous structure, which resulted in the best interfacial charge transfer on Bi catalyst [46, 78, 79]. It can imply that the increased potential is attributed to the decrease in R_{CT} [78].

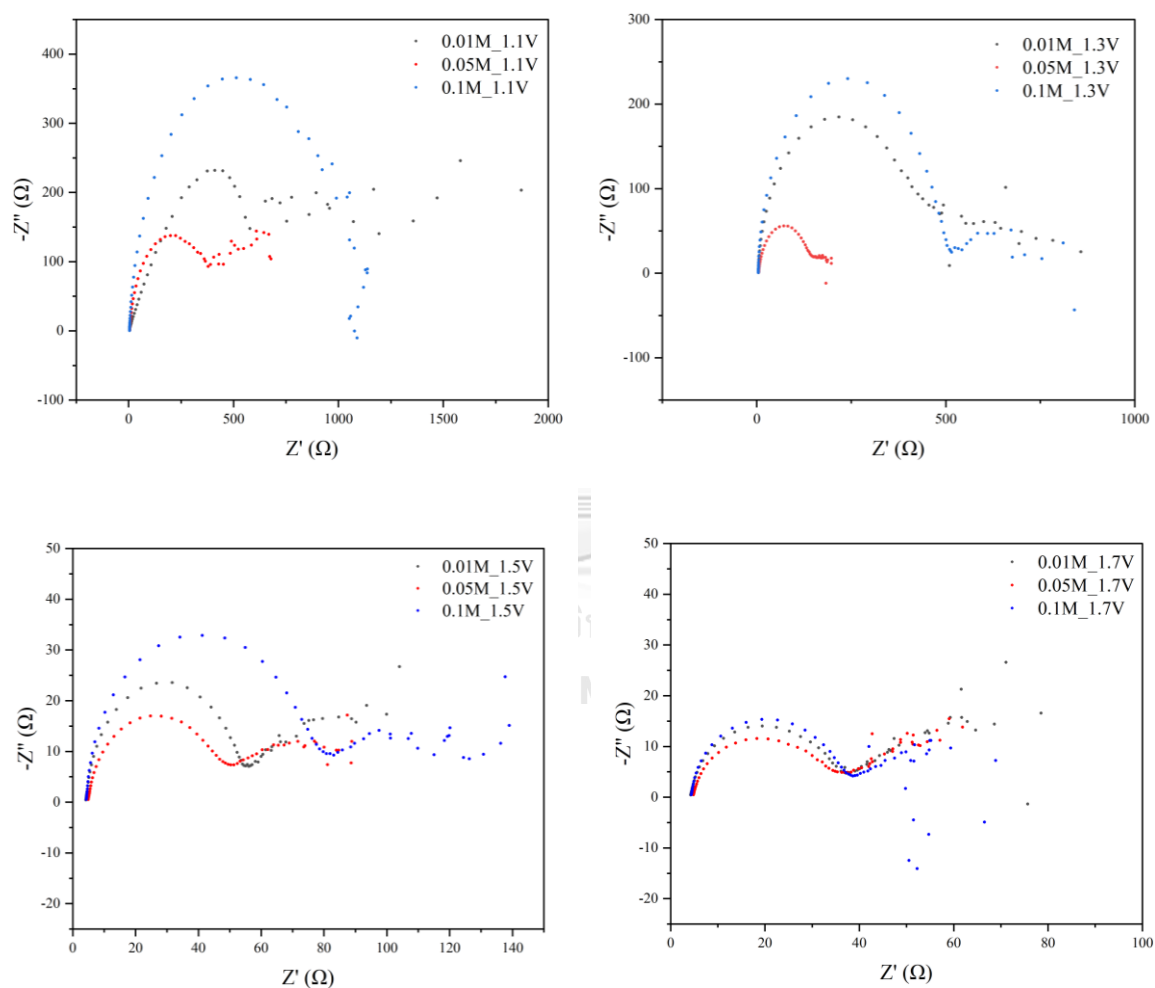


Figure 22. EIS result of Bi/Sn electrode

Table 9. Charge-transfer resistances of Bi/Sn electrocatalyst prepared in several Bi concentration bath.

Bi Concentration (M)	R_{ct} (charge-transfer resistances) (Ω)			
	-1.1 V	-1.3 V	-1.5 V	-1.7 V
0.01	597.48	477.61	51.96	33.23
0.05	392.77	144.40	46.04	31.89
0.1	1015.44	516.42	78.68	34.41

4.4 CO₂RR performance test on electrocatalysts prepared in various Bi concentrations bath

The CO₂RR experiments were studied using the Bi/Sn electrodes prepared with 0.01 M – 0.1 M Bi concentration at -1.1 V vs. Ag/AgCl for 70 min. The SEM-EDX, TEM-EDX-SAED, and XPS techniques were used to analyze the electrodes and the solid products. GC analyzed the gas products. The liquid products were analyzed using NMR.

4.4.1 SEM-EDX analysis

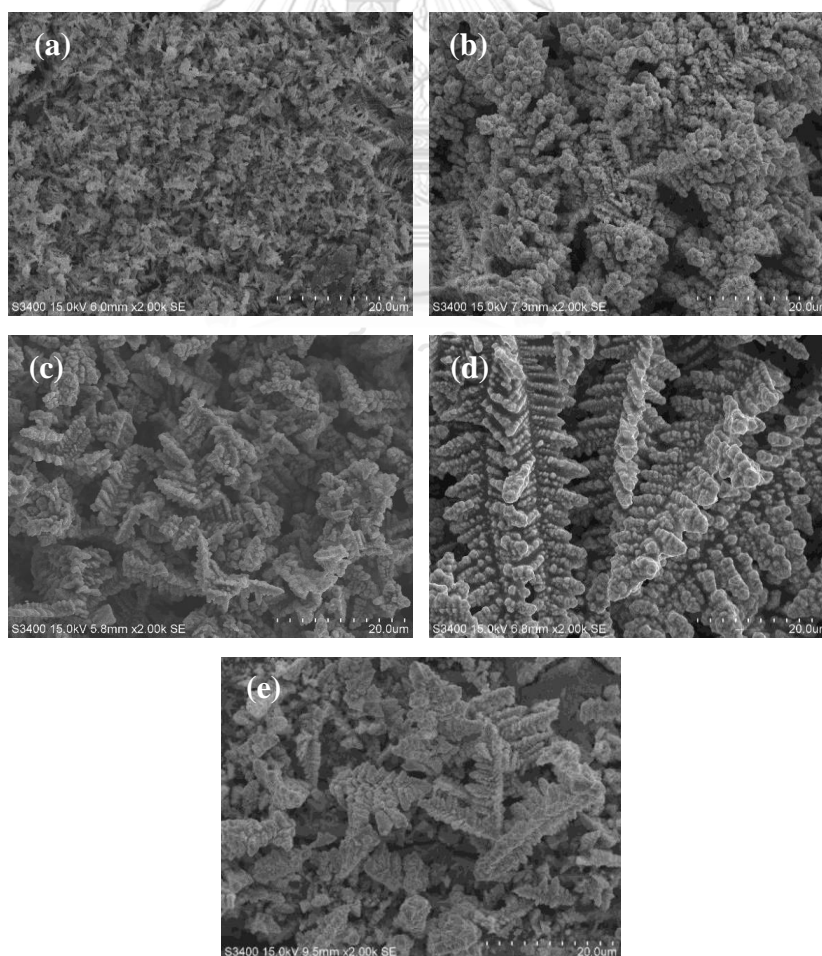


Figure 23. SEM images after CO₂RR at -1.1 V : (a) 0.01 M (b) 0.03 M (c) 0.05 M (d) 0.07 M and (e) 0.1 M Bi concentration on Sn electrode

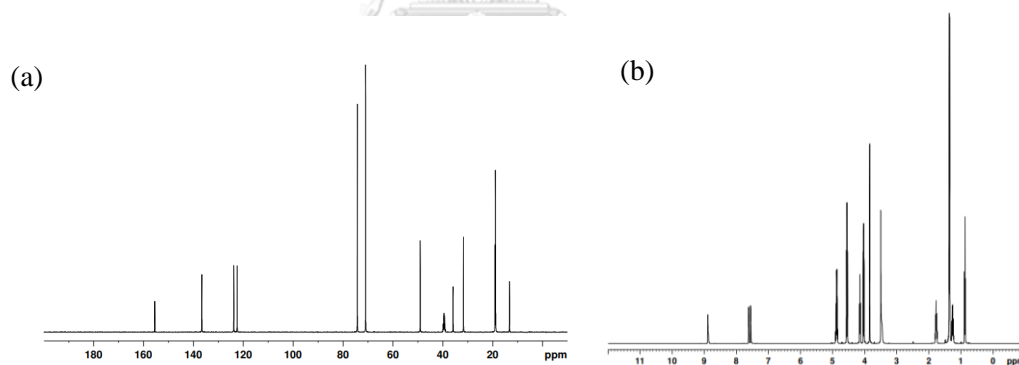
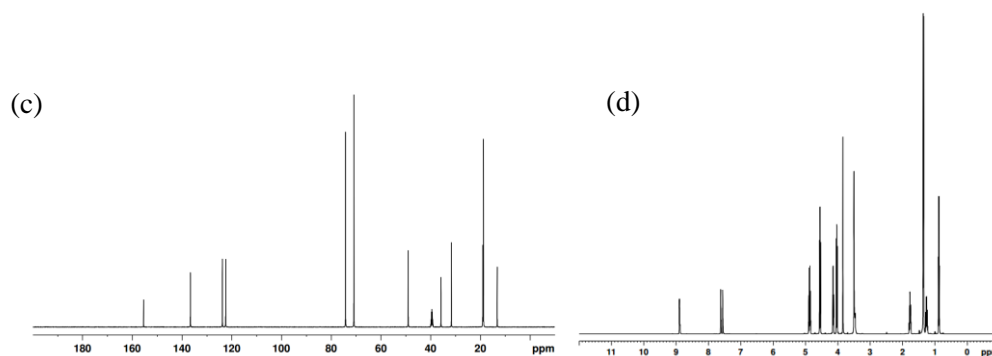
Table 10. The EDX result after CO₂RR at -1.1 V for 70 min.

Catalyst	The percent by atom (%)				
	Bi (%)	Sn (%)	F (%)	O (%)	C (%)
0.01Bi/Sn	40.24	7.38	12.18	16.90	23.29
0.03Bi/Sn	41.98	8.68	11.27	16.98	21.09
0.05Bi/Sn	25.91	6.52	17.75	17.07	32.74
0.07 Bi/Sn	18.84	4.22	22.35	10.84	43.74
0.1Bi/Sn	15.97	19.68	11.63	32.08	20.64

From the SEM-EDX results, the morphology of all Bi/Sn electrodes prepared in various Bi concentrations bath after CO₂RR at -1.1 V vs. Ag/AgCl for 70 min showed that the Bi dendrite structure was retained. However, the size of the dendrite was smaller than before CO₂RR. This is because the outer electrode surface is loosened during the reaction [80].

4.4.2 GC and NMR analysis

Under all conditions and electrocatalysts, neither gaseous nor liquid products were found, as verified by the GC and NMR results.

**Figure 24.** NMR result of electrolyte: (a) ¹³C NMR (b) ¹H NMR**Figure 25.** NMR result of all concentrations: (a) ¹³C NMR (b) ¹H NMR

4.4.3 Raman analysis

As shown in Figure 26, the Raman results demonstrate that the D and G bands in Raman spectroscopy were attributed to the carbon products formed [16]. The carbon products were obtained at 0.03 M, 0.05 M, 0.07 M, and 0.1 M Bi concentrations by the mechanism of Rungkiat et al. 2022 [16]. The Raman spectra corresponding to the solid carbon products showed two deconvoluted peaks centered at around 1366 and 1566 cm^{-1} , which are defined as graphene products from D and G bands around 1350 and 1580 cm^{-1} , respectively [81, 82]. Comparing the Raman spectra of the carbon product on the Bi/Sn electrodes prepared in 0.03 M, 0.05 M, 0.07 M, and 0.1 M Bi concentration bath, the range of 0.05 M – 0.07 M Bi concentration promoted more carbon products than the others.

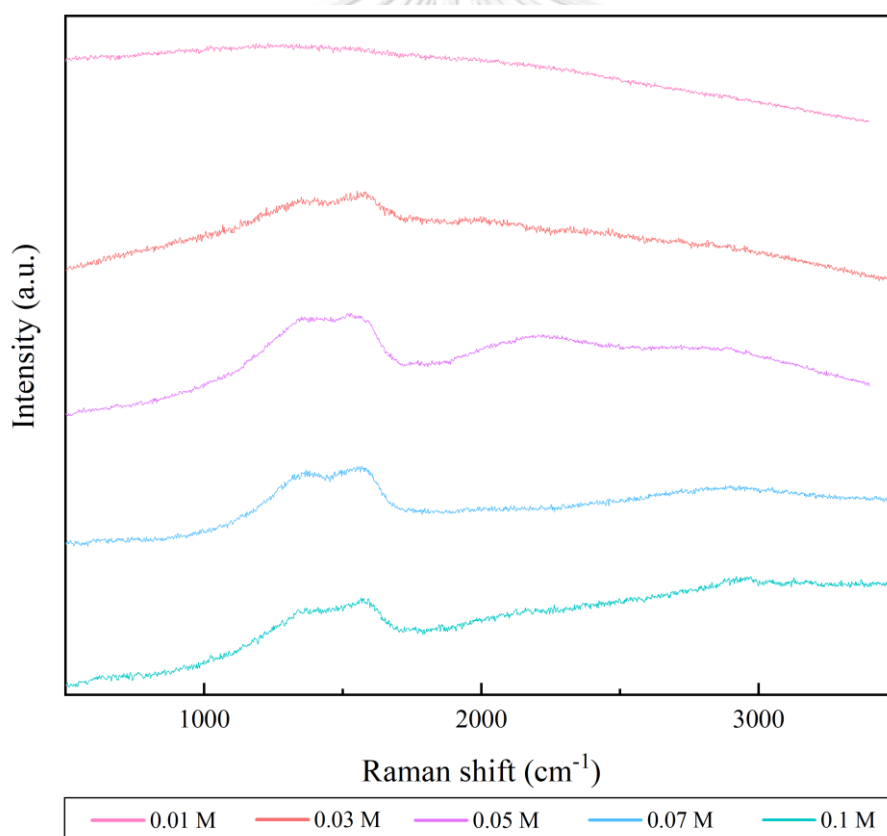


Figure 26. Raman results of the Bi/Sn electrodes after CO_2RR reaction at -1.1 V vs. Ag/AgCl for 70 min

4.4.4 TEM-EDX-SAED analysis

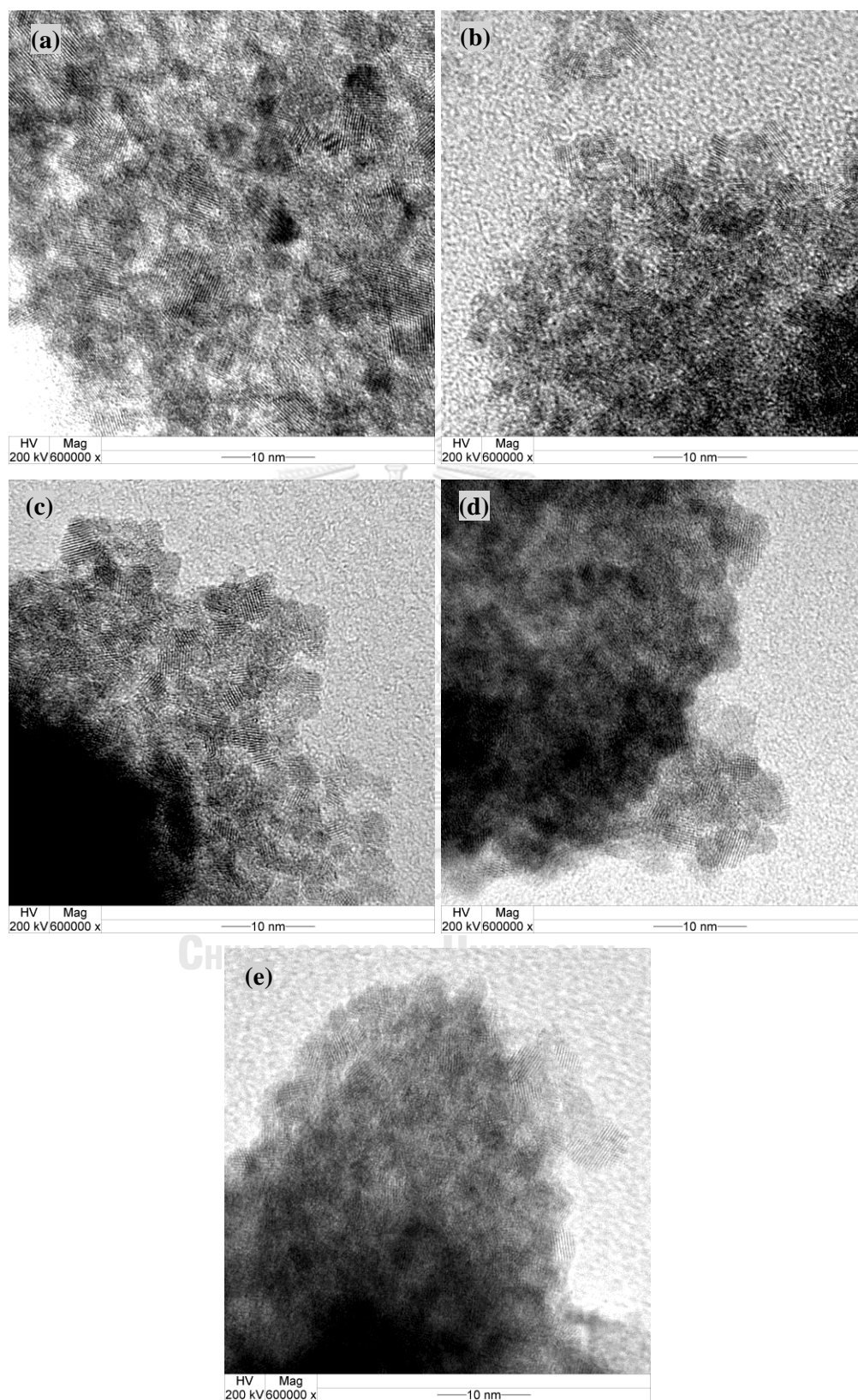


Figure 27. TEM : (a) 0.01 M (b) 0.03 M (c) 0.05 M (d) 0.07 M (e) 0.1 M Bi/Sn electrode after CO₂RR at -1.1 V vs. Ag/AgCl for 70 min

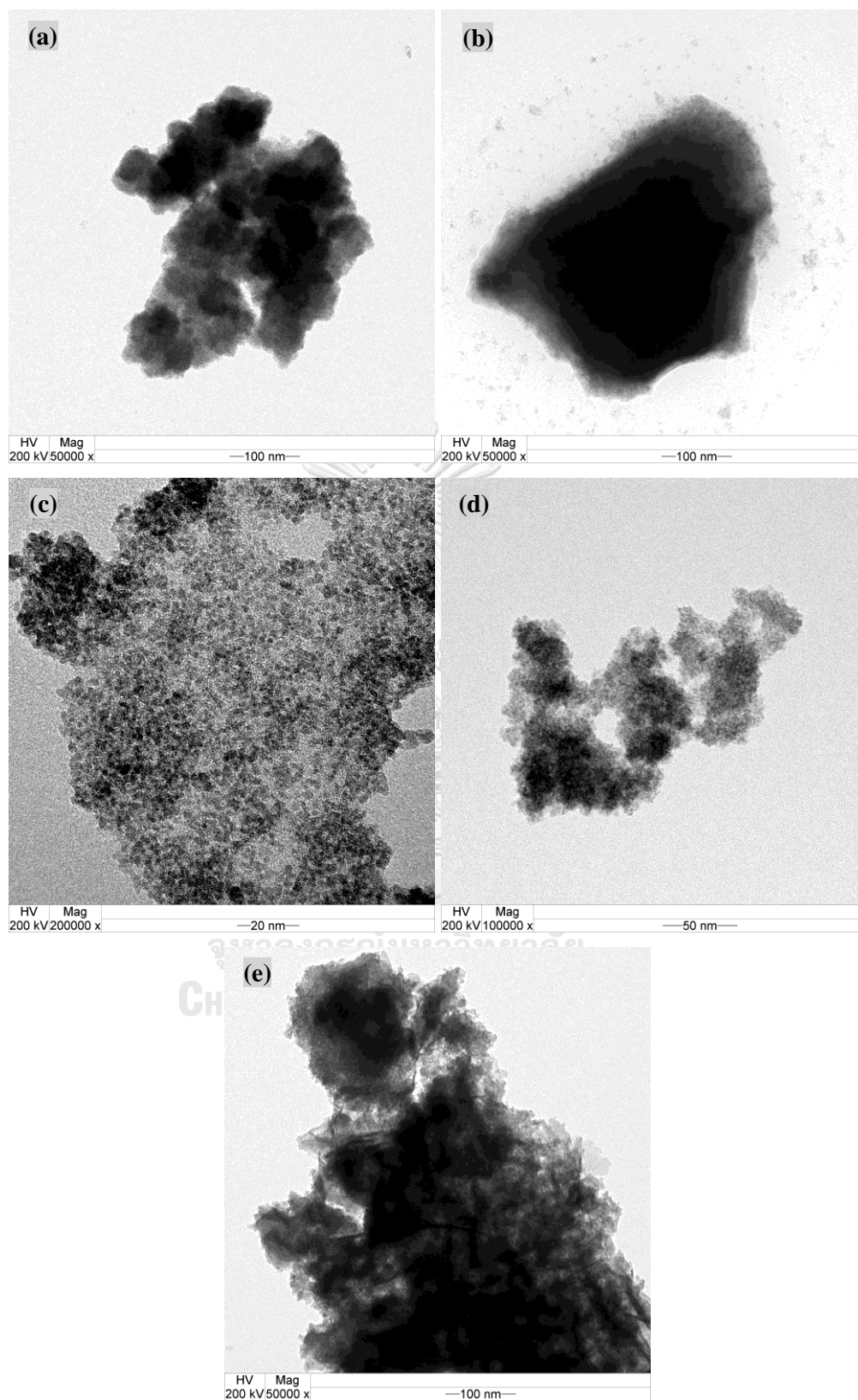


Figure 28. TEM-EDX results : (a) 0.01 M (b) 0.03 M (c) 0.05 M (d) 0.07 M (e) 0.1 M Bi/Sn electrode after CO₂RR at -1.1 V vs. Ag/AgCl for 70 min

Table 11. TEM-EDX results of Bi/Sn electrode after CO₂RR at -1.1 V for 70 min

Catalyst	The percent by atom (%)				
	Bi (%)	Sn (%)	F (%)	O (%)	C (%)
0.01Bi/Sn	0.49	12.11	1.59	36.05	49.75
0.03Bi/Sn	0.00	17.53	6.11	31.29	45.06
0.05Bi/Sn	0.50	4.66	1.28	21.90	71.65
0.07 Bi/Sn	0.24	6.84	0.62	17.09	75.21
0.1Bi/Sn	9.44	8.83	0.00	32.20	49.53

TEM-EDX-SAED was used to confirm carbon products from the Raman and SEM-EDX results. In Figure 27, the images reveal single-crystalline fringes in the nanometric range with an average crystallite domain size of approximately 3 nm [16]. All Bi/Sn electrodes exhibit d-spacing around 0.258 nm, which show the SAED patterns of the Bi (111) plane [16]. Bi (111) surface is the most stable surface and natural cleavage plane of Bi single crystals; hence, the (111) characteristic planes of the nanocrystalline carbon products were formed as anticipated [83].

The TEM-EDX results in Figure 28 and Table 11 reveal a high carbon element of up to 70%. The SAED pattern of the Bi/Sn electrodes were analyzed. The d-spacing (Å) from the SAED patterns of the particles on the 0.05Bi/Sn and 0.1Bi/Sn electrodes matched the graphite pattern [84]. The results of d-spacing (Å) propose graphite-3R (Rhombohedral) from JCPDS26-1079, in which the pattern was found around 3.35 Å (003), 2.01 Å (101), 1.96 Å (012), 1.67 Å (006), 1.62 Å (104) and 1.46 Å (015) [16]. The results of d-spacing matching with graphite confirmed Raman results that the carbon product was polycrystalline graphene.

4.4.5 XPS analysis

XPS characterization was used to investigate the surface chemical states of the electrocatalysts of the 0.03Bi/Sn, 0.07Bi/Sn electrodes surface after CO₂RR at -1.1 V vs. Ag/AgCl for 70 min. The XPS results are shown in Figures 29 and 30. In Figure 29, the Bi 4f peak around binding energy 159 eV and 164 eV represent Bi 4f_{7/2} and Bi 4f_{5/2} [70, 71], respectively. The result of Bi 4f_{7/2} and Bi 4f_{5/2} refer to Bi³⁺ species in Bi oxide [72]. On the 0.07Bi/Sn electrode, the main peak of the XPS results found binding energy at 157 and 162 eV, which refers to metallic Bi⁰. This result happened

from a high Bi concentration on the electrode due to the form high and tall dendrite structure. It can suggest that Bi^{3+} reduces to Bi^0 or the outer electrode surface during the reaction as the oxide layer is loosened during the reaction, which corresponds to the SEM-EDX result after CO_2RR [70, 71].

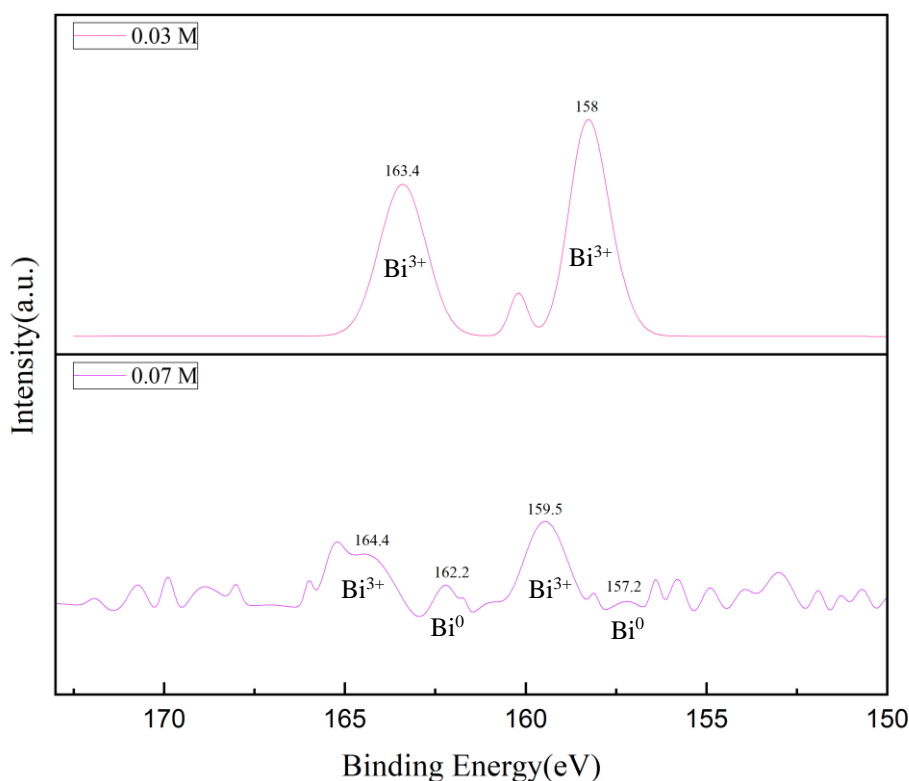


Figure 29. Bi 4f XPS spectra image of Bi/Sn electrodes after CO_2RR at -1.1 V

In Figure 30, the XPS spectra exhibit the binding energy at 285 eV, which refers to the sp^3 C-C group [85, 86]. For the 0.03 Bi/Sn electrode, The XPS spectrum found binding energy at 283.9 eV, which refers to the sp^2 C=C group [87, 88]. These results confirm Raman's result and TEM results that carbon products are polycrystalline graphene. However, C-OH groups with XPS binding energies at 286.4 eV were also detected on the 0.07 M samples, suggesting the formation of graphene oxide after the reaction [85, 89, 90].

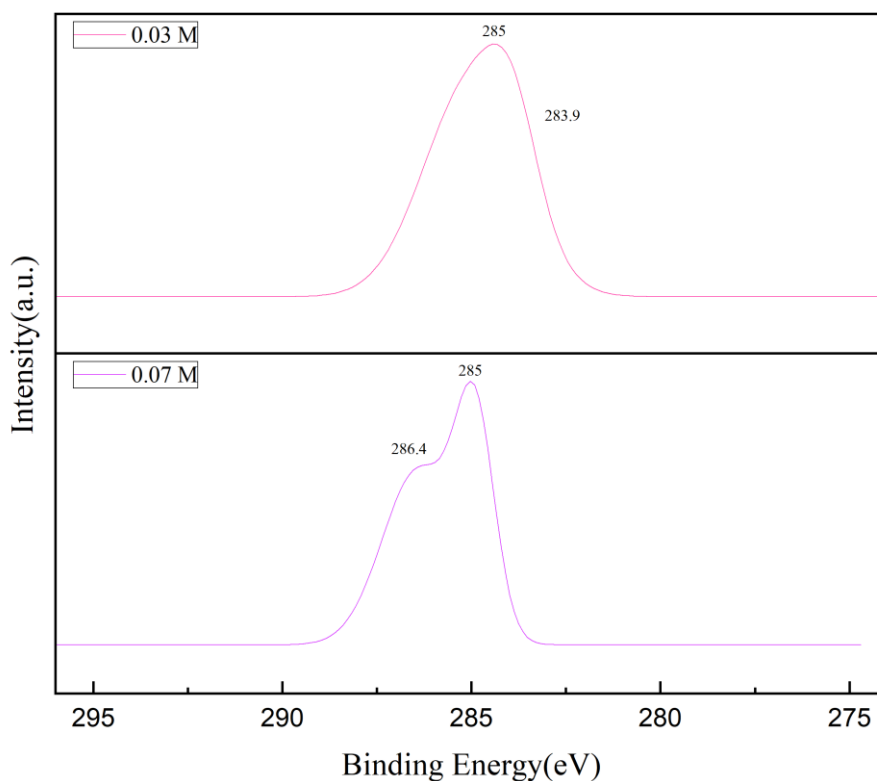


Figure 30. C1s XPS spectra image of the Bi/Sn electrodes after CO₂RR at -1.1 V

From the results in part 1, the suitable Bi concentration in synthesizing Bi/Sn electrocatalyst for CO₂RR at -1.1 V vs. Ag/AgCl for 70 min in [BMIM]BF₄/ PC/DI electrolyte was 0.05 M. The Raman, SEM-EDX, TEM, and XPS results showed polycrystalline graphene as a solid carbon product. The highest carbon product was observed on the electrocatalysts prepared in the Bi concentration bath ranging from 0.05 M to -0.07 M. However, The 0.05Bi/Sn electrode was selected to further study in part 2 because of their lower required bismuth precursor.

Part 2: To study the suitable potential for the CO₂RR performance to produce carbon allotropes in [BMIM]BF₄/ PC/DI electrolyte.

4.5 Potential for the CO₂RR at 70 min

The CO₂RR was further investigated for 70 minutes using 0.05 Bi/Sn electrodes at varied applied potentials ranging from -1.1 to -1.7 V vs. Ag/AgCl.

4.5.1 SEM-EDX analysis

From the SEM-EDX result, the morphology of 0.05Bi/Sn electrode after CO₂RR at all potentials for 70 min showed that the dendrite structure was retained. However, the size of the dendrite was decreased after CO₂RR. This is because the outer electrode surface lost during the reaction [80].

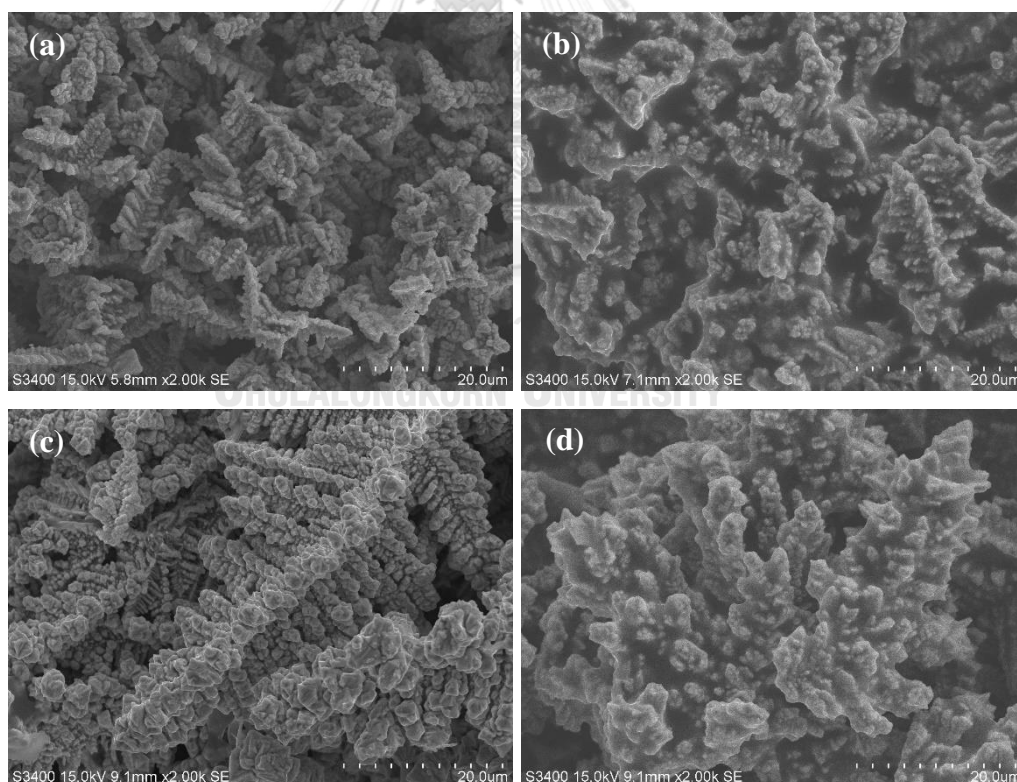


Figure 31. SEM images of 0.05 Bi/Sn after CO₂RR for 70 min : (a)-1.1 V (b) -1.3 V (c) -1.5 V (d) -1.7 v

Table 12. The EDX result of 0.05 Bi/Sn electrode after CO₂RR for 70 min.

Applied potential (V vs. Ag/AgCl)	The percent by atom (%)				
	Bi (%)	Sn (%)	F (%)	O (%)	C (%)
-1.1 V.	25.91	6.52	17.75	17.07	32.74
-1.3 V.	6.16	5.58	27.17	10.07	51.01
-1.5 V.	24.38	6.94	14.97	14.70	39.01
-1.7 V.	7.48	6.37	23.58	13.42	49.14

4.5.2 GC and NMR analysis

According to the NMR results, no liquid products were produced for any of the applied potentials. From GC results, gas products were found as CO and H₂ in the system. Figure 8 and Table 1 show the mechanism of CO production and the equation of CO and H₂ in CO₂RR and HER, respectively. When the potential was raised, the CO product increased with the applied potential at -1.5 V vs. Ag/AgCl show the highest CO product. Further increase of applied potential to -1.7 V vs. Ag/AgCl, CO decreased and H₂ product increased by HER at the relatively negative potential.

Table 13. The gas products of CO₂RR on 0.05Bi/Sn electrode at various applied potentials for 70 min.

Potential (V)	faradaic efficiency (FE, %)	
	H ₂	CO
-1.1	0.00	0.00
-1.3	0.00	0.16
-1.5	0.00	0.56
-1.7	3.01	0.50

4.5.3 Raman analysis

From the Raman results (Figure 32), the graphene products were confirmed by the D and G bands around 1350 and 1580 cm⁻¹ [81, 82]. The Raman bands corresponding to the graphene products increased with increasing potential from -1.1 to -1.3 V vs. Ag/AgCl. The carbon peak intensity decreased when the potential increased to -1.5 V and -1.7 V vs. Ag/AgCl. Thus, the most effective potential for CO₂RR to solid carbon product on the 0.05Bi/Sn electrode was determined to be at -1.3 V vs. Ag/AgCl, with a small amount of CO by-product. The best effective

potential for CO₂RR to solid carbon product on the 0.05Bi/Sn electrode was discovered to be -1.3 V vs. Ag/AgCl.

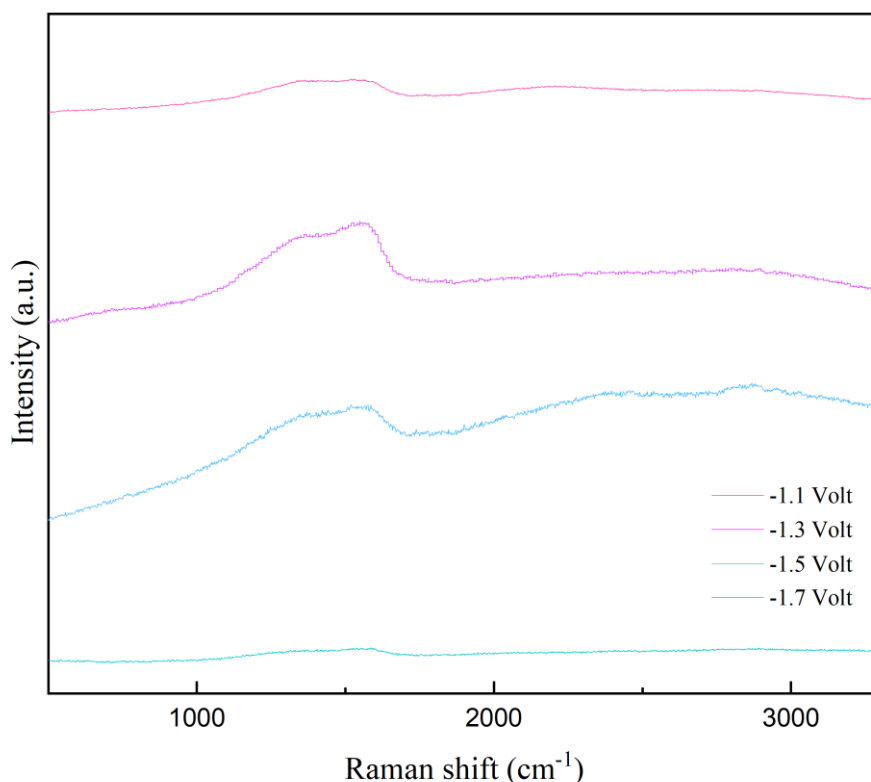


Figure 32. Raman results of the 0.05Bi/Sn electrode after CO₂RR reaction at -1.1 to -1.7 V vs. Ag/AgCl for 70 min by using 0.05 M Bi/Sn electrode

According to the CO₂RR findings, a substantial amount of CO product was formed with the lowest carbon products at the highest applied potential (-1.7 V vs. Ag/AgCl). In addition, H₂ evolution, which is a competitive reaction to CO₂RR took place. Furthermore, almost half of the Bi on the Sn electrode separated from the electrode into the electrolyte during the reaction due to the high amount of gaseous products. It can suggest that -1.7 V vs. Ag/AgCl was the highest voltage limit for the use of Bi/Sn electrode in the CO₂RR reaction under [BMIM]BF₄/PC/DI system.

From the results, the optimum potential conditions for high performance production of 0.05Bi/Sn electrode in CO₂RR toward solid carbon products under the [BMIM]BF₄/PC/DI electrolyte system were applied potential of -1.3 V vs. Ag/AgCl.

4.6 The stability test of CO₂RR on 0.05Bi/Sn electrode for 150 min.

The CO₂RR was further studied for 150 minutes on the 0.05Bi/Sn electrode at applied potentials -1.3 V vs. Ag/AgCl under [BMIM]BF₄/PC/DI system,

4.6.1 SEM-EDX analysis

From the SEM-EDX result, the morphology of 0.05 Bi/Sn electrode after CO₂RR at -1.3 V vs. Ag/AgCl. For 70 and 150 min showed that the dendrite structure was retained. However, the size of the dendrite was smaller than before CO₂RR. This is because the outer electrode surface is loosened during the reaction [80]. And EDX result showed a ratio of Bi: C; Reconstruction of Bi as electrocatalyst is any change of chemical composition from CO₂RR [91, 92].

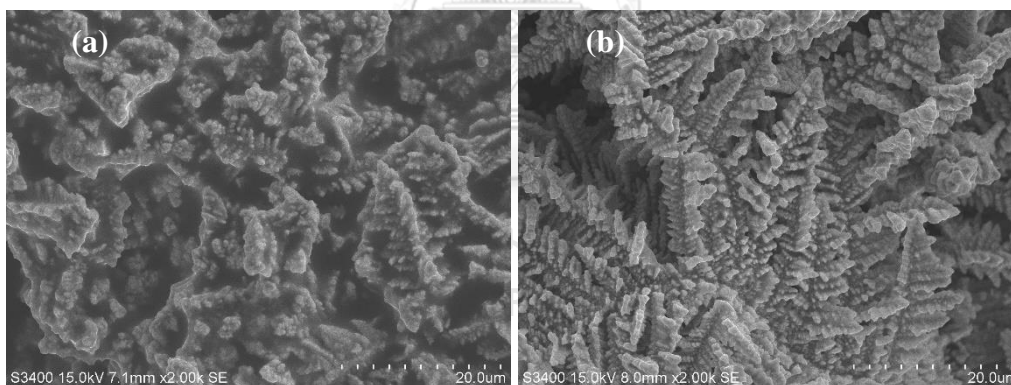


Figure 33. SEM image of 0.05 Bi/Sn after CO₂RR (a) 70 min (b) 150 min

Table 14. The EDX result after CO₂RR at 0.05 Bi/Sn -1.3 V

Catalyst	The percent by atom (%)				
	Bi (%)	Sn (%)	F (%)	O (%)	C (%)
70 min	6.16	5.58	27.17	10.07	51.01
150 min	23.67	5.84	17.51	10.92	42.13

4.6.2 GC and NMR analysis

From the NMR results, no liquid products were found under both conditions, for 70 and 150 min. Table 15 shows the GC results, the highest CO product was observed at 30 min (FE=0.42%) and then decreased. The GC results at 70 min and 150 min show the same tendency.

Table 15. The gas products of CO₂RR on 0.05Bi/Sn electrode at -1.3 V for 150 min. faradaic efficiency (FE, %)

Time (min)	faradaic efficiency (FE, %)	
	H ₂	CO
0	0.00	0.00
30	0.00	0.42
60	0.00	0.18
90	0.00	0.12
120	0.00	0.00
150	0.00	0.00

4.6.3 Raman analysis

As shown in Figure 34, the Raman results, the graphene products were confirmed by the D and G bands around 1350 and 1580 cm⁻¹[81, 82]. The Raman bands correspond to the highest graphene products at -1.3 V vs. Ag/AgCl on a 0.05Bi/Sn electrode for 70 min. At 150 min, It showed graphene product decrease when compared with 70 min because of reconstruction of Bi, which corresponds to the results of SEM-EDX result.

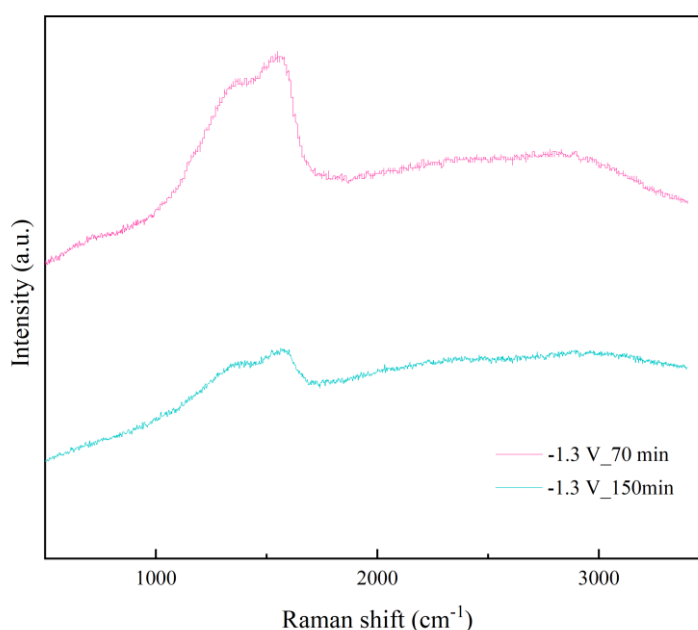


Figure 34. Raman results of the Bi/Sn electrodes after CO₂RR reaction at -1.3 V vs. Ag/AgCl for 70 and 150 min by using 0.05 M Bi/Sn electrode

From the finding, to produce high performance of Bi/Sn electrode in CO₂RR toward solid carbon products under the [BMIM]BF₄/PC/DI electrolyte system, the optimum time conditions were 70 min, applied potential -1.3 V vs. Ag/AgCl using 0.05 M Bi concentration on Sn electrode.



CHAPTER V

CONCLUSIONS

5.1 Conclusions

The CO₂RR is a viable negative CO₂ emission method to convert CO₂ gas into value-added solid carbon material while reducing the source of the greenhouse effect that causes the world climate change crisis. In this research, Bi a non-toxic and common material was selected as the electrocatalyst for CO₂RR towards solid carbon products. The effect of Bi concentration (0.01 M, 0.03 M, 0.05 M, 0.07 M, and 0.1 M) during the electrodeposition of Bi³⁺ on Sn foil on the properties of the Bi/Sn electrodes was studied. The CO₂RR performances of the prepared electrodes were evaluated at various applied potentials under the [BMIM]BF₄/PC/DI electrolyte system. From SEM-EDX analysis, the dendrite structure was formed on the electrode surface after electrodeposition. The XPS results showed an oxide layer of Bi³⁺ on the electrode surface for all the electrocatalysts. The EIS results found that the 0.05Bi/Sn electrode had the lowest charge-transfer resistance, which makes it a promising effective electrocatalyst for CO₂RR. The use of 0.05 Bi/Sn to 0.07 Bi/Sn electrodes show high performance in CO₂RR toward solid carbon products at -1.1 V vs. Ag/AgCl. The carbon product was analyzed as polycrystalline graphene according to TEM/EDX, XPS, and Raman spectroscopy. The appropriate potential for CO₂RR under the [BMIM]BF₄/PC/DI electrolyte system was -1.3 V vs. Ag/AgCl for 70 min to provide the highest performance in CO₂RR to the solid carbon product.

5.2 Recommendation

5.2.1. The Bi/Sn electrode performance in this system should be studied between 0.05-0.07 M Bi concentration range.

5.2.2. Further analysis should be performed on the XRD to characterize material properties like crystal structure, crystallite size, and strain on the electrode surface for all concentrations.

5.2.3. The electrochemically active surface area (ECSA) is used to find the active surface area on the electrode surface by using the CV experiment at a different scan rate in the potential range of non-reaction [93, 94]. Appendix B. shows the results of CV on the Bi/Sn electrode in CO₂RR under the [BMIM]BF₄/PC/DI electrolyte. It showed that the result couldn't find the range of potential for non-reaction in this system. Therefore, it suggests changing electrolytes from ionic liquid groups to the aqueous group.

5.2.4. The effect of the amount of Bi would be further investigated. The previous research has studied the effect of the increased amount of metal ions by increasing concentration due to an increase in the rate of electrodeposition [95]. Another research has studied about the effect to structure. However, as the metal ion increase, The structure does not change shape, and the size of the structure will be larger and taller [28, 67, 96]. The size of the structure depends on the amount of metal ions [40]. The mass transfer will decrease when concentration increases, affecting the mass transfer coefficient [97].

5.2.5. The quantitatively of the carbon product should be investigated by conversion of CO₂. The conversion of CO₂ will calculate from the weighing of the before and after electrodes. Before weighing the electrode, the electrode should be dry by using the dehumidifying oven.

5.2.6. The purity of carbon product formation would be further investigated and developed for this system. The previous research has studied the reduced graphene oxide on metal at the electrode surface by using the electrochemical exfoliation method to separate the outer layers of the deposited film [98]. Then, separate the graphene product and the electrolyte by using the filter and following the oven to dry

and give the powder of graphene [99]. Another previous research has studied to reduce graphene oxide on Bi oxide electrodes to increase electrode surface area by using thermal decomposition in a muffle stove [100].

5.2.7. The application of nanocrystalline graphene would be studied.



REFERENCES

References

1. Yang, D., Q. Zhu, and B. Han, Electroreduction of CO₂ in Ionic Liquid-Based Electrolytes. *The Innovation*, 2020. **1**(1): p. 100016.
2. Faggion, D., W.D.G. Gonçalves, and J. Dupont, CO₂ Electroreduction in Ionic Liquids. *Frontiers in Chemistry*, 2019. **7**(102).
3. Navarro-Jaén, S., et al., Highlights and challenges in the selective reduction of carbon dioxide to methanol. *Nature Reviews Chemistry*, 2021. **5**(8): p. 564-579.
4. DiMeglio, J.L. and J. Rosenthal, Selective Conversion of CO₂ to CO with High Efficiency Using an Inexpensive Bismuth-Based Electrocatalyst. *Journal of the American Chemical Society*, 2013. **135**(24): p. 8798-8801.
5. Medina-Ramos, J., J.L. DiMeglio, and J. Rosenthal, Efficient Reduction of CO₂ to CO with High Current Density Using in Situ or ex Situ Prepared Bi-Based Materials. *Journal of the American Chemical Society*, 2014. **136**(23): p. 8361-8367.
6. Fedotov, A., et al., Electrodeposition conditions-dependent crystal structure, morphology and electronic properties of Bi films. *Journal of Alloys and Compounds*, 2021. **887**: p. 161451.
7. Kuppusami, P. and V.S. Raghunathan, Status of pulsed laser deposition: challenges and opportunities. *Surface Engineering*, 2006. **22**(2): p. 81-83.
8. Grabov, V.M., et al., Size effect in galvanomagnetic phenomena in bismuth films doped with tellurium. *Semiconductors*, 2014. **48**(5): p. 630-635.
9. Fedotov, A.S., et al., Temperature dynamics of the electronic structure in dilute Bi-Sn alloys. *Physical Review B*, 2018. **97**(7): p. 075204.
10. Ávila-Bolívar, B., et al., Electrochemical Reduction of CO₂ to Formate on Easily Prepared Carbon-Supported Bi Nanoparticles. *Molecules*, 2019. **24**(11): p. 2032.
11. Atifi, A., et al., Directing the Outcome of CO₂ Reduction at Bismuth Cathodes Using Varied Ionic Liquid Promoters. *ACS Catalysis*, 2018. **8**(4): p. 2857-2863.
12. Wen, G., et al., Orbital Interactions in Bi-Sn Bimetallic Electrocatalysts for Highly Selective Electrochemical CO₂ Reduction toward Formate Production. *Advanced Energy Materials*, 2018. **8**(31): p. 1802427.
13. Li, Q., et al., Novel Bi, BiSn, Bi₂Sn, Bi₃Sn, and Bi₄Sn Catalysts for Efficient Electroreduction of CO₂ to Formic Acid. *Industrial & Engineering Chemistry Research*, 2020. **59**(15): p. 6806-6814.
14. Sanjuán, I., et al., Bi-Sn nanoparticles for electrochemical denitrification: activity and selectivity towards N₂ formation. *Electrochimica Acta*, 2020. **340**: p. 135914.
15. Li, Z., et al., Fabrication of Bi/Sn bimetallic electrode for high-performance electrochemical reduction of carbon dioxide to formate. *Chemical Engineering Journal*, 2022. **428**: p. 130901.
16. Nganglumpoon, R., et al., Growing 3D-nanostructured carbon allotropes from CO₂ at room temperature under the dynamic CO₂ electrochemical reduction environment. *Carbon*, 2022. **187**: p. 241-255.
17. Zhu, Q., et al., Efficient Reduction of CO₂ into Formic Acid on a Lead or Tin

- Electrode using an Ionic Liquid Catholyte Mixture. *Angewandte Chemie International Edition*, 2016. **55**(31): p. 9012-9016.
18. Sharifi Golru, S. and E.J. Biddinger, Effect of additives in aqueous electrolytes on CO₂ electroreduction. *Chemical Engineering Journal*, 2022. **428**: p. 131303.
 19. Wang, C., et al., Tuning the Basicity of Ionic Liquids for Equimolar CO₂ Capture. *Angewandte Chemie International Edition*, 2011. **50**(21): p. 4918-4922.
 20. Oh, Y. and X. Hu, Ionic liquids enhance the electrochemical CO₂ reduction catalyzed by MoO₂. *Chemical Communications*, 2015. **51**(71): p. 13698-13701.
 21. Li, F., et al., Ionic liquids for CO₂ electrochemical reduction. *中国化学工程学报*, 2021. **29**(3): p. 75-93.
 22. Gonçalves, W.D.G., et al., Efficient Electrocatalytic CO₂ Reduction Driven by Ionic Liquid Buffer-Like Solutions. *ChemSusChem*, 2019. **12**(18): p. 4170-4175.
 23. Wu, M., et al., Electrochemical reduction of CO₂ to carbon films on stainless steel around room temperature. *Electrochemistry Communications*, 2020. **110**: p. 106606.
 24. Esrafilzadeh, D., et al., Room temperature CO₂ reduction to solid carbon species on liquid metals featuring atomically thin ceria interfaces. *Nature Communications*, 2019. **10**: p. 865.
 25. Liu, S., et al., Enhanced Electrocatalytic CO₂ Reduction of Bismuth Nanosheets with Introducing Surface Bismuth Subcarbonate. *Coatings*, 2022. **12**(2): p. 233.
 26. Moretto, L.M., et al., Pyrolyzed Photoresist Carbon Electrodes for Trace Electroanalysis of Nickel(II). *Chemosensors*, 2015. **3**: p. 157-168.
 27. Darayen, J., et al., Porous Electrodeposited Cu as a Potential Electrode for Electrochemical Reduction Reactions of CO₂. *Applied Sciences*, 2021. **11**(23): p. 11104.
 28. Grujicic, D. and B. Pesic, Electrodeposition of copper: the nucleation mechanisms. *Electrochimica Acta*, 2002. **47**(18): p. 2901-2912.
 29. Zhang, X., et al., Electrocatalytic carbon dioxide reduction: from fundamental principles to catalyst design. *Materials Today Advances*, 2020. **7**: p. 100074.
 30. Tylar Greene, P.J. 2021 Tied for 6th Warmest Year in Continued Trend, NASA Analysis Shows. 2022; Available from: <https://climate.nasa.gov/news/3140/2021-tied-for-6th-warmest-year-in-continued-trend-nasa-analysis-shows/>.
 31. Buis, A. A Degree of Concern: Why Global Temperatures Matter. 2019; Available from: <https://climate.nasa.gov/news/2865/a-degree-of-concern-why-global-temperatures-matter>.
 32. 2021, U.C.c.c.U. COP26. 2021; Available from: <https://ukcop26.org/>.
 33. TEAM, E.M.I. Carbon Markets Rocket in 2021, On Track to Break \$1B for First Time. 2021; Available from: <https://www.ecosystemmarketplace.com/articles/press-release-voluntary-carbon-markets-rocket-in-2021-on-track-to-break-1b-for-first-time/Voluntary>
 34. Zhang, L., Z.-J. Zhao, and J. Gong, Nanostructured Materials for Heterogeneous Electrocatalytic CO₂ Reduction and their Related Reaction Mechanisms. *Angewandte Chemie International Edition*, 2017. **56**(38): p. 11326-11353.
 35. Topham, S., et al., Carbon Dioxide. 2014. p. 1-43.
 36. Zhang, W., et al., Progress and Perspective of Electrocatalytic CO₂ Reduction

- for Renewable Carbonaceous Fuels and Chemicals. *Advanced Science*, 2018. **5**(1): p. 1700275.
37. Jung, H., et al., Electrochemical Fragmentation of Cu₂O Nanoparticles Enhancing Selective C–C Coupling from CO₂ Reduction Reaction. *Journal of the American Chemical Society*, 2019. **141**(11): p. 4624-4633.
 38. Pei, Y., H. Zhong, and F. Jin, A brief review of electrocatalytic reduction of CO₂ —Materials, reaction conditions, and devices. *Energy Science & Engineering*, 2021. **9**.
 39. Zangari, G., Fundamentals of Electrodeposition, in *Encyclopedia of Interfacial Chemistry*, K. Wandelt, Editor. 2018, Elsevier: Oxford. p. 141-160.
 40. Sobha Jayakrishnan, D., 5 - Electrodeposition: the versatile technique for nanomaterials, in *Corrosion Protection and Control Using Nanomaterials*, V.S. Saji and R. Cook, Editors. 2012, Woodhead Publishing. p. 86-125.
 41. Moura de Salles Pupo, M. and R. Kortlever, Electrolyte Effects on the Electrochemical Reduction of CO₂. *ChemPhysChem*, 2019. **20**(22): p. 2926-2935.
 42. Shukla, S.K., et al., Ionic Liquids: Potential Materials for Carbon Dioxide Capture and Utilization. *Frontiers in Materials*, 2019. **6**.
 43. Hollingsworth, N., et al., Reduction of Carbon Dioxide to Formate at Low Overpotential Using a Superbase Ionic Liquid. *Angewandte Chemie International Edition*, 2015. **54**(47): p. 14164-14168.
 44. Rudnev, A.V., et al., Enhanced electrocatalytic CO formation from CO₂ on nanostructured silver foam electrodes in ionic liquid/water mixtures. *Electrochimica Acta*, 2019. **306**: p. 245-253.
 45. Vasilyev, D.V., et al., A General and Facile Approach for the Electrochemical Reduction of Carbon Dioxide Inspired by Deep Eutectic Solvents. *ChemSusChem*, 2019. **12**(8): p. 1635-1639.
 46. Ju, F., J. Zhang, and W. Lu, Efficient Electrochemical Reduction of CO₂ to CO in Ionic Liquid/Propylene Carbonate Electrolyte on Ag Electrode. *Catalysts*, 2020. **10**(10): p. 1102.
 47. Zhang, L., et al., Imidazolium Ions with an Alcohol Substituent for Enhanced Electrocatalytic Reduction of CO₂. *ChemSusChem*, 2017. **10**(24): p. 4824-4828.
 48. Koh, J.H., et al., Oxygen Plasma Induced Hierarchically Structured Gold Electrocatalyst for Selective Reduction of Carbon Dioxide to Carbon Monoxide. *The Journal of Physical Chemistry C*, 2015. **119**(2): p. 883-889.
 49. Fu, Y., et al., Surface Structure Sensitivity of CO₂ Electroreduction on Low-Index Gold Single Crystal Electrodes in Ionic Liquids. *ChemElectroChem*, 2018. **5**(5): p. 748-752.
 50. Chen, T.-Y., et al., Selection of Low-Cost Ionic Liquid Electrocatalyst for CO₂ Reduction in Propylene Carbonate/Tetrabutylammonium Perchlorate. *ChemElectroChem*, 2018. **5**(16): p. 2295-2300.
 51. Zhou, F., et al., Highly selective and stable electro-catalytic system with ionic liquids for the reduction of carbon dioxide to carbon monoxide. *Electrochemistry Communications*, 2015. **55**: p. 43-46.
 52. Koh, J.H., et al., Facile CO₂ Electro-Reduction to Formate via Oxygen Bidentate Intermediate Stabilized by High-Index Planes of Bi Dendrite Catalyst. *ACS Catalysis*, 2017. **7**(8): p. 5071-5077.

53. Castillo, A., et al., Sn nanoparticles on gas diffusion electrodes: Synthesis, characterization and use for continuous CO₂ electroreduction to formate. *Journal of CO₂ Utilization*, 2017. **18**: p. 222-228.
54. Medina-Ramos, J., et al., Efficient Conversion of CO₂ to CO Using Tin and Other Inexpensive and Easily Prepared Post-Transition Metal Catalysts. *Journal of the American Chemical Society*, 2015. **137**(15): p. 5021-5027.
55. Zhang, X., et al., Electrochemical Reduction of Carbon Dioxide to Formic Acid in Ionic Liquid [Emim][N(CN)₂]/Water System. *Electrochimica Acta*, 2017. **247**: p. 281-287.
56. Feng, J., et al., Insights into Carbon Dioxide Electroreduction in Ionic Liquids: Carbon Dioxide Activation and Selectivity Tailored by Ionic Microhabitat. *ChemSusChem*, 2018. **11**(18): p. 3191-3197.
57. Wu, H., et al., Design of naturally derived lead phytate as an electrocatalyst for highly efficient CO₂ reduction to formic acid. *Green Chemistry*, 2018. **20**.
58. Chen, L., et al., Electrochemical Reduction of CO₂ at Metal Electrodes in a Distillable Ionic Liquid. *ChemSusChem*, 2016. **9**(11): p. 1271-1278.
59. Ding, C., et al., In Situ Electrodeposited Indium Nanocrystals for Efficient CO₂ Reduction to CO with Low Overpotential. *ACS Catalysis*, 2016. **6**(10): p. 6438-6443.
60. Atifi, A., et al., Insights into the Composition and Function of a Bismuth-Based Catalyst for Reduction of CO₂ to CO. *The Journal of Physical Chemistry C*, 2019. **123**(14): p. 9087-9095.
61. Zhang, Z., et al., Rational Design of Bi Nanoparticles for Efficient Electrochemical CO₂ Reduction: The Elucidation of Size and Surface Condition Effects. *ACS Catalysis*, 2016. **6**(9): p. 6255-6264.
62. Sun, X., et al., Molybdenum–Bismuth Bimetallic Chalcogenide Nanosheets for Highly Efficient Electrocatalytic Reduction of Carbon Dioxide to Methanol. *Angewandte Chemie International Edition*, 2016. **55**(23): p. 6771-6775.
63. Kunene, T., A. Atifi, and J. Rosenthal, Selective CO₂ Reduction over Rose's Metal in the Presence of an Imidazolium Ionic Liquid Electrolyte. *ACS Applied Energy Materials*, 2020. **3**(5): p. 4193-4200.
64. Nadjo, L. and J.M. Savéant, Linear sweep voltammetry: Kinetic control by charge transfer and/or secondary chemical reactions: I. Formal kinetics. *Journal of Electroanalytical Chemistry and Interfacial Electrochemistry*, 1973. **48**(1): p. 113-145.
65. Instruments, G., Basics of electrochemical impedance spectroscopy. G. Instruments, *Complex impedance in Corrosion*, 2007: p. 1-30.
66. Kuhl, K., et al., New insights into the electrochemical reduction of carbon dioxide on metallic copper surfaces. *Energy & Environmental Science*, 2012. **5**: p. 7050-7059.
67. Zhang, T., et al., Bi-Modified Zn Catalyst for Efficient CO₂ Electrochemical Reduction to Formate. *ACS Sustainable Chemistry & Engineering*, 2019. **7**(18): p. 15190-15196.
68. Wu, J., et al., Dendrite-Free Zinc-Based Battery with High Areal Capacity via the Region-Induced Deposition Effect of Turing Membrane. *Journal of the American Chemical Society*, 2021. **143**(33): p. 13135-13144.
69. Lu, W., et al., Inhibition of Zinc Dendrite Growth in Zinc-Based Batteries.

- ChemSusChem, 2018. **11**(23): p. 3996-4006.
70. Dubuis, S., et al., The effect of Bi₂O₃ on the physical, structural and NIR emission properties of BGG glasses prepared at different melting atmospheres. *Optical Materials Express*, 2021. **11**.
 71. Dharmadhikari, V.S., et al., Characterisation of thin films of bismuth oxide by X-ray photoelectron spectroscopy. *Journal of Electron Spectroscopy and Related Phenomena*, 1982. **25**(2): p. 181-189.
 72. Zatsepin, D.A., et al., Bi-doped silica glass: A combined XPS – DFT study of electronic structure and pleomorphic imperfections. *Journal of Alloys and Compounds*, 2020. **829**: p. 154459.
 73. Tao, J.G., et al., Origin of XPS binding energy shifts in Ni clusters and atoms on rutile TiO₂ surfaces. *Surface Science*, 2008. **602**: p. 2769-2773.
 74. Jiang, H., et al., High-selectivity electrochemical CO₂ reduction to formate at low overpotential over Bi catalyst with hexagonal sheet structure. *Applied Surface Science*, 2021. **541**: p. 148577.
 75. Zhang, G., et al., Bi⁵⁺, Bi(3-x)⁺, and Oxygen Vacancy Induced BiOCl_xI_{1-x} Solid Solution toward Promoting Visible-Light Driven Photocatalytic Activity. *Chemistry – A European Journal*, 2018. **24**(29): p. 7434-7444.
 76. Zalecki, R., et al., Bismuth Valence in a Ti_{0.7}Bi_{0.3}Sr_{1.6}Ba_{0.4}CaCu₂O_y Superconductor from X-Ray Photoemission Spectroscopy. *Acta Physica Polonica A*, 2010. **118**: p. 393-395.
 77. Lv, C., et al., Oxygen-Induced Bi⁵⁺-Self-Doped Bi₄V₂O₁₁ with a p-n Homojunction Toward Promoting the Photocatalytic Performance. *ACS Applied Materials & Interfaces*, 2017. **9**(28): p. 23748-23755.
 78. Choi, W., et al., Modeling and Applications of Electrochemical Impedance Spectroscopy (EIS) for Lithium-ion Batteries. *J. Electrochem. Sci. Technol*, 2020. **11**(1): p. 1-13.
 79. Ye, S., et al., Mimicking the Key Functions of Photosystem II in Artificial Photosynthesis for Photoelectrocatalytic Water Splitting. *Journal of the American Chemical Society*, 2018. **140**(9): p. 3250-3256.
 80. Morimoto, M., et al., Electrodeposited Cu-Sn Alloy for Electrochemical CO₂ Reduction to CO/HCOO. *Electrocatalysis*, 2018. **9**.
 81. Childres, I., et al., Raman spectroscopy of graphene and related materials. *New developments in photon and materials research*, 2013. **1**: p. 1-20.
 82. Malard, L.M., et al., Raman spectroscopy in graphene. *Physics Reports*, 2009. **473**(5): p. 51-87.
 83. Oh, W., et al., Atomic and Molecular Adsorption on the Bi(111) Surface: Insights into Catalytic CO₂ Reduction. *The Journal of Physical Chemistry C*, 2018. **122**(40): p. 23084-23090.
 84. Esmeryan, K., et al., Kinetically driven graphite-like to diamond-like carbon transformation in low temperature laminar diffusion flames. *Diamond and Related Materials*, 2017. **75**.
 85. Ma, C., et al., Facile Synthesis of Reduced Graphene Oxide/Fe₃O₄ Nanocomposite Film. *Journal of Applied Biomaterials & Functional Materials*, 2017. **15**(1_suppl): p. 1-6.
 86. Al-Gaashani, R., et al., XPS and structural studies of high quality graphene oxide and reduced graphene oxide prepared by different chemical oxidation

- methods. *Ceramics International*, 2019. **45**(11): p. 14439-14448.
87. Gao, G., et al., Heat-Initiated Chemical Functionalization of Graphene. *Scientific Reports*, 2016. **6**: p. 20034.
 88. Park, J., et al., Observation of the intrinsic bandgap behaviour in as-grown epitaxial twisted graphene. *Nature communications*, 2015. **6**: p. 5677.
 89. Dwivedi, N., et al., Understanding the Role of Nitrogen in Plasma-Assisted Surface Modification of Magnetic Recording Media with and without Ultrathin Carbon Overcoats. *Scientific reports*, 2015. **5**: p. 7772.
 90. Zhao, F., et al., Graphene-Nanodiamond Heterostructures and their application to High Current Devices. *Scientific Reports*, 2015. **5**.
 91. Kui, K., et al., Dynamic Surface Chemistry of Catalysts in Oxygen Evolution Reaction. *Small Science*, 2021. **1**.
 92. Yao, D., et al., The Controllable Reconstruction of Bi-MOFs for Electrochemical CO₂ Reduction through Electrolyte and Potential Mediation. *Angewandte Chemie International Edition*, 2021. **60**.
 93. Trasatti, S. and O.A. Petrii, Real surface area measurements in electrochemistry. *Journal of Electroanalytical Chemistry*, 1992. **327**(1): p. 353-376.
 94. Alia, S., et al., Mercury Underpotential Deposition to Determine Iridium and Iridium Oxide Electrochemical Surface Areas. *Journal of The Electrochemical Society*, 2016. **163**: p. F3051-F3056.
 95. Kumar, S., S. Pande, and P. Verma, Factor effecting electro-deposition process. *International Journal of Current Engineering and Technology*, 2015. **5**(2): p. 700-703.
 96. Das, A. and M. Sangaranarayanan, Shape-controlled synthesis of three-dimensional triangular bismuth microstructures and sensing of H₂O₂. *CrystEngComm*, 2016. **18**(7): p. 1147-1155.
 97. Sedahmed, G.H., Y.A. El-Taweel, and O.A. Hassan, The role of mass transfer in the kinetics of the electrodeposition of metal powder at gas-evolving electrodes. *Surface Technology*, 1981. **14**(2): p. 109-117.
 98. Li, Y., et al., Electrodeposition of reduced graphene oxide onto gold electrodes: creating thin electrochemically active and optically transparent overlayers. *Electrochimica Acta*, 2019. **319**: p. 649-656.
 99. Ni Htwe, Y., M. Jaafar, and S. Chin, Fabrication of Graphene by Electrochemical Intercalation Method and Performance of Graphene/PVA Composites as Stretchable Strain Sensor. *Arabian Journal for Science and Engineering*, 2020. **45**.
 100. Ciszewski, M., et al., Reduced graphene oxide–bismuth oxide composite as electrode material for supercapacitors. *Ionics*, 2015. **21**(2): p. 557-563.



จุฬาลงกรณ์มหาวิทยาลัย
CHULALONGKORN UNIVERSITY

VITA

NAME Ms.Sarita Phupaichitkun

DATE OF BIRTH 19 April 1997

PLACE OF BIRTH Thailand

INSTITUTIONS ATTENDED Bachelor of Engineering (B.Eng.In chemical engineering),
Chemical Engineering King Mongkut's Institute of
Technology Ladkrabang, Thailand,2018

HOME ADDRESS 158/3 Soi Inthamara 26/1 Suthisarn Road, Din Daeng,
Ratchada Pisek, Bangkok, 10400.



จุฬาลงกรณ์มหาวิทยาลัย
CHULALONGKORN UNIVERSITY